2009

Carbon Dioxide Flooding Induced Geochemical Changes in a Saline Carbonate Aquifer

Alyssa Boock
University of North Dakota

CARBON DIOXIDE FLOODING INDUCED GEOCHEMICAL CHANGES IN A SALINE CARBONATE AQUIFER

by

Alyssa Boock

Bachelor of Science in Geology, University of Wisconsin-River Falls, 2002

A Thesis

Submitted to the Graduate Faculty

of the

University of North Dakota

in partial fulfillment of the requirements

for the degree of

Master of Science

Grand Forks, North Dakota

December
2009

This thesis, submitted by Alyssa Boock in partial fulfillment of the requirements for the Degree of Master of Science from the University of North Dakota, has been read by the Faculty Advisory Committee under whom the work has been done and is hereby approved.

_____
Chairperson

_____

_____

This thesis meets the standards for appearance, conforms to the style and format requirements of the Graduate School of the University of North Dakota, and is hereby approved.

_____
Dean of the Graduate School

_____
Date

PERMISSION

Title Carbon Dioxide Flooding Induced Geochemical Changes in a Saline Carbonate Aquifer

Department Geology

Degree Master of Science

In presenting this thesis in partial fulfillment of the requirements for a graduate degree from the University of North Dakota, I agree that the library of this University shall make it freely available for inspection. I further agree that permission for extensive copying for scholarly purposes may be granted by the professor who supervised my thesis work or, in his absence, by the chairperson of the department or the dean of the Graduate School. It is understood that any copying or publication or other use of this thesis or part thereof for financial gain shall not be allowed without my written permission. It is also understood that due recognition shall be given to me and to the University of North Dakota in any scholarly use which may be made of any material in my thesis.

Signature _____

Date _____

TABLE OF CONTENTS

LIST OF FIGURES

LIST OF TABLES

ACKNOWLEDGMENTS

I would like to extend my sincerest thanks and appreciation to my committee chairman Dr. Zheng-Wen (Zane) Zeng for his guidance, support, and willingness to work with me as an off-campus student. I would also like to thank my other committee members, Dr. Scott Korom and Dr. Richard LeFever, for their help, suggestions, and guidance with this project.

This research was generously funded by the US Department of Energy through contracts DE-FC26-05NT42592 and DE-FC26-08NT0005643 and by North Dakota Industry Commission (NDIC) together with Encore Acquisition Company, Hess Corporation, Marathon Oil Company, St. Mary Land & Exploration Company, and Whiting Petroleum Corporation under contract NDIC-G015-031.

I would like to thank Xue Jun (John) Zhou and Hong Liu for their assistance with the operation of the core-flooding system and rock core preparation. Hanying Xu, director of UND's Environmental Analytical Research Laboratory, provided instruction and guidance with the laboratory instruments. Dr. Robert Baker has provided guidance and encouragement since I was a child, and helped push me into geology and eventually graduate school. I would also like to thank my past and present employers for allowing me to schedule my work around my schooling when needed.

Finally I would like to thank my family and friends for their support and encouragement through my coursework at UND and my return to finish. A special thanks goes to Tanya Justham for her support and friendship during my return.

ABSTRACT

Carbon dioxide (CO_2) has been injected into depleted oil reservoirs for enhanced oil recovery for several decades. Injection of CO_2 into geologic formations in the Williston Basin is currently under consideration for long-term CO_2 storage to reduce anthropogenic CO_2 emissions to the atmosphere. The Madison Group in the North Dakota Williston Basin provides the greatest potential for geologic sequestration in either deep saline aquifers or depleted oil reservoirs. Little is known about the geochemical reactions that take place when supercritical carbon dioxide is injected into deep saline aquifers at geologic conditions similar to those found in potential sequestration units of the Madison Group.

Previous studies have shown the injection of carbon dioxide into a saline aquifer makes the formation water slightly acidic, which reacts with the host rock to dissolve carbonate minerals. Dissolution of carbonate minerals may compromise the integrity of the formation, leading to the eventual escape of CO_2 to the surface. In order for CO_2 sequestration to be effective, CO_2 must remain below the surface indefinitely. Studies of the properties of carbon dioxide indicate that CO_2 is less soluble with increasing salinity, resulting in less carbonate dissolution. Formation waters in Madison Group aquifers range in salinity from 1,000 ppm to greater than 300,000 ppm total dissolved solids. Sodium chloride (NaCl) is the primary salt of the formation waters of the Madison Group. Water-alternating-gas (WAG) flooding experiments were conducted on

limestone rock cores using a core flooding system that simulates the CO_2 injection process at subsurface conditions. Deionized (DI) water and three different concentrations of NaCl solutions, 1,000 ppm, 10,000 ppm and 100,000 ppm were used to represent salinities found in the formation waters in the Madison Group in the Williston Basin.

Effluent water was collected for analysis of pH, specific conductance, sodium, calcium, iron, chloride, alkalinity and total dissolved solids. The presence of calcium, and to a lesser extent, alkalinity and decreased pH and in the effluent samples, indicate limestone dissolution took place throughout the flooding experiments at all water flood concentrations. Calcium and alkalinity concentrations were highest during the 100,000 ppm flooding and lowest during the deionized water flooding, indicating CO_2 is more soluble with increasing salinities at geologic conditions found in the aquifers of the Madison Group in the North Dakota Williston Basin than was previously reported.

CHAPTER 1

INTRODUCTION

Carbon dioxide (CO_2) has been injected into depleted oil reservoirs for enhanced oil recovery (EOR) since the 1970s (Solomon et al., 2008). CO_2 displaces petroleum and can provide up to 40% more recovery as a tertiary means of oil recovery after primary production and secondary water flooding (Blunt et al., 1993).

With levels of greenhouse gases rising, increased effort is being focused on ways to effectively inject carbon dioxide into geologic formations for long-term storage (sequestration) to reduce anthropogenic carbon dioxide emissions to the atmosphere (USDOE, 2002). Atmospheric greenhouse gas levels have risen 30%, at a steady rate of 1-2 ppm/year since the industrial revolution began in the 18^{th} century, suggesting a large impact from anthropogenic sources (USDOE, 2002). Projected levels of greenhouse gas are expected to rise 33% over the next 20 years (USDOE, 2002). CO_2 currently represents 83% of greenhouse gas, the majority is likely a result of anthropogenic activities (USDOE, 2002). Enting et al. (2008) developed a model to determine the benefits of lowering CO_2 levels to the atmosphere by CO_2 storage in geologic formations. Provided there is little leakage of CO_2 back to the atmosphere, the model predicts a decrease in the average worldwide temperature of approximately 2.5°C over the next 100 years with an overall benefit dependent on the amount of CO_2 captured and stored (Enting et al., 2008).

Several studies have been conducted to estimate the effectiveness of different means of CO_2 storage in geologic formations. Proposed geologic media for CO_2 storage are deep saline aquifers (van der Meer, 1993; Bergman and Winter, 1995; Holloway, 1997), depleted oil and gas reservoirs (Blunt et al., 1993; USDOE, 2002; Nelms and Burke, 2004; Fischer et al., 2005a, b, c; Solomon et al., 2008), and unmineable coal seams (Bachu, 2000; USDOE, 2002). Of these methods, saline aquifers offer the greatest potential for storage of large volumes of CO_2 (Bachu, 2000; Gaus et al., 2008; Birkholzer et al., 2009) and many are located in the same sedimentary basins as fossil fuels (Hitchon et al., 1999; Bachu, 2000; Giammar et al., 2008). However, depleted hydrocarbon reservoirs might be the most economically viable due to the presence of infrastructure already in place and proceeds from enhanced oil recovery offsetting the cost of additional infrastructure (Holt et al., 1995; Hitchon et al., 1999; Pawar et al., 2002).

Little is known about the geochemical reactions that take place when supercritical CO_2 is injected into deep saline aquifers at geologic conditions similar to those found in potential sequestration units of the Williston Basin in North Dakota. The Madison Group provides the greatest potential for geologic sequestration in either deep saline aquifers or depleted oil reservoirs (Fischer et al., 2005c). The Madison Group contains the Lodgepole and Mission Canyon limestones overlain by the Charles Formation evaporites; all of which were deposited during the Mississippian (Heck, 1979; Fischer et al., 2005a). Total dissolved solids (TDS) in formation waters of the Madison aquifer range from 1,000 ppm to greater than 300,000 ppm (Downey, 1984; Busby et al., 1995). Depth to the top of the Madison is over 2200 meters (m), which is much deeper than the minimum 800 m required for CO_2 sequestration (Holloway and Savage, 1993; van der Meer, 1993;

Nelms and Burke, 2004; Solomon et al., 2008). Pressures, temperatures and salinities found in the Madison Group are generally higher than those found in previously conducted experiments and at large-scale projects. CO_2 will be in its supercritical state at these geologic conditions in the Madison Group.

Previous studies have shown that the injection of CO_2 into a saline aquifer makes the formation waters slightly acidic, which react with the host rock to dissolve the carbonate minerals in the rock (Emberley et al., 2005; Kaszuba et al., 2005; Ketzer et al., 2009). Studies of the properties of carbon dioxide indicate CO_2 is less soluble with increasing salinity (Carr et al., 2003; Duan and Sun, 2003).

Core flooding experiments were conducted to determine the geochemical changes that take place during water-alternating-gas (WAG) injections under simulated geologic conditions of the Madison Group of the North Dakota Williston Basin. Limestone cores were subjected to injections of brine of different salinities to represent various formation water salinities that might be encountered in various aquifers or oil fields of the Madison Group. It was unknown how the core flooding system would react with high salinity water; therefore, the tests covered the lower range of salinities found in the Williston Basin, including 1,000 ppm, 10,000 ppm, and 100,000 ppm NaCl solutions.

Each rock core was subjected to 5 WAG cycles for a total of 3000 ml combined CO_2 and H_2O injected. In addition to the three saline solutions, one rock core was flooded with deionized (DI) water for baseline data.

It is predicted that CO_2 will react with the saline water to form carbonic acid and dissolve calcite minerals in the limestone. The acidic solution is predicted to dissolve the rock along the injection channel, and dissolved calcium and carbonate species will be

found in the effluent waters. However, less dissolution of limestone will take place with increasing water salinity, resulting in fewer dissolved calcium and carbonate ions in the effluent with increasing salinity. In addition, as a result of dissolution, rock core porosity will increase.

All effluent water samples were analyzed for pH, specific conductance, calcium, sodium, iron, chloride, bicarbonate alkalinity and total dissolved solids to determine any changes in the water chemistry after undergoing WAG injections through a carbonate rock sample. The limestone rock used in the experiments was the Indiana Limestone, an industry standard, which has been previously reported at approximately 98-99% pure calcium carbonate ($CaCO_3$) (McGee, 1989).

CHAPTER II

BACKGROUND

Carbon Dioxide Storage Mechanisms

The goal of carbon sequestration is to trap (sequester) the carbon dioxide, or otherwise limit its mobility (storage), making it unlikely to leak back to the surface. Several storage mechanisms exist to effectively trap CO_2, including structural and stratigraphic trapping, mineral trapping, residual trapping, hydrodynamic trapping, and solution trapping (Bachu, 2003; Giammar et al., 2005; Bachu et al., 2007).

Structural trapping involves anticlines, domes, faults and other geologic structures that impede the vertical and horizontal migration, and potential escape of CO_2. Stratigraphic trapping refers to the restriction of fluid movement provided by strata seals, such as low permeability evaporite beds. Depleted oil and gas reservoirs have previously demonstrated integrity of geologic structures needed to trap fluids and gases (Hitchon et al., 1999; USDOE, 2002; Solomon et al., 2008). Some oil and gas fields at or near maturity occur in structural traps.

Mineral trapping is considered to be the ultimate method for CO_2 sequestration by trapping CO_2 in crystal structures as new minerals precipitate from solution. This process takes the longest time, on the order of hundreds to thousands of years, but is the most likely to sequester CO_2 for geologic time (Gunter et al., 1997; Hitchon et al., 1999; Bachu et al., 2007). Several small-scale experiments have shown new carbonate minerals

precipitate after chemical reactions between the formation water, rock, and CO_2 result in excess ions in solution from dissolution of the host rock and/or divalent cations from the brine. (Bachu et al., 1994; Soong et al., 2004; Xu et al., 2004; Giammer et al., 2005). As NaCl brine has no divalent cations, carbonate mineral precipitation is more likely to occur after reaction with silicate minerals (Kaszuba et al., 2005).

Residual trapping occurs when CO_2 injection displaces formation water and/or other fluids and occupies the pore space originally taken up by the formation water. When CO_2 injection ceases, displaced water flows back around the injection point, trapping CO_2 in the pores (Taku Ide, 2007; Solomon et al., 2008).

Hydrodynamic trapping occurs when the mobility of CO_2 injected into deep saline aquifers is limited due to extremely slow flow rates of formation waters. CO_2 gas is more buoyant than the denser formation water and will flow up-dip over time. The distance for some deep aquifers to discharge can be very large, resulting in residence times of thousands to millions of years, by which time the CO_2 may have participated in mineral trapping (Bachu et al., 1994; Bachu, 2000; Solomon et al., 2008).

Solution trapping occurs when high temperatures and pressures found in deep aquifers allow CO_2 to partially dissolve into the formation waters. Up to 29% of injected CO_2 can be dissolved in the formation water (Bachu et al., 1994; Law and Bachu, 1996). CO_2 saturated formation water is denser (approximately 1%) than the surrounding formation water, resulting in the loss of buoyancy and sinking within the aquifer (Solomon et al., 2008). CO_2 becomes trapped in solution because the buoyancy forces driving CO_2 upward are lost due to increased pressures and temperatures at the greater depth.

Concerns about changes in the rock structure as a result of CO_2 injection have led to several experiments and numerical modeling (Wier et al., 1995; Gaus et al., 2002; Xu et al., 2004; Izgec et al., 2008; Zhou et al., 2009). There are generally two schools of thought regarding the behavior of injected CO_2: reservoir engineering, where CO_2 displaces formation waters (Birkholzer et al., 2009; Zhou et al., 2008a), and dissolution, where CO_2 dissolves into formation waters (Holloway and Savage, 1993; Bachu and Adams, 2003; Qi et al., 2009). More accurately, it is a combination of both (Gunter et al., 2000; Andre et al., 2007). Some of the CO_2 dissolves into the formation waters and some remains as a separate phase, which can displace formation waters. If CO_2 is injected into aquifers at a high rate, pressure can build up, causing the rocks to fracture or faults to reactivate (Zhou et al., 2008b; Oruganti and Bryant, 2009) which may lead to CO_2 escape. Chemical reactions between the host rock, formation water, and CO_2 may alter the porosity, permeability and strength of the rock structure. (Gaus et al., 2008).

Carbon Dioxide at Deep Geologic Conditions

The chemical properties of CO_2 have been studied for several centuries and basic properties of CO_2 are well known. CO_2 reaches the critical point at 31.1°C and 7.38 MPa (Bachu, 2000). At temperatures and pressures above the critical point, CO_2 is in its supercritical state where it behaves like a gas but has the density of a liquid. Based on an average thermal gradient of 25°C/km, supercritical temperature would occur at a depth of around 800 m in geologic formations. Overburden fluid pressure equal to the supercritical pressure occurs at about the same depth, based on an average hydrostatic pressure gradient of 1 MPa/100 m (Holloway and Savage, 1993). At depths shallower than 800 m, carbon dioxide exists as a compressed gas, with density less than the

formation water, resulting in buoyancy driving the CO_2 gas upwards. Conditions near the injection point allow for CO_2 injection in its supercritical state, but as CO_2 migrates away from the injection point, changing conditions may allow for CO_2 to return to its gaseous state. Behavior of CO_2 in deep, saline aquifers is not well known. Several experimental studies (Shiraki and Dunn, 2000; Kaszuba et al., 2003, 2005; Yang et al., 2008) and numerical modeling (Weir et al., 1995; Allen et al., 2005; Lagneau et al., 2005; Spycher and Preuss, 2005) have been conducted to better understand interactions of CO_2 with brine and host rock at conditions related to geologic CO_2 sequestration.

Deep aquifers contain saline formation waters (Gaus et al., 2008; Solomon et al., 2008). CO_2 solubility increases with increasing pressure but decreases with increasing temperature and salinity (Holloway and Savage, 1993; Holt et al., 1995; Izgec et al., 2008). CO_2 solubility in formation waters at 100,000 ppm salinity is approximately 70% of the solubility in fresh water (Carr et al., 2003). Several experiments have shown that both carbonate (limestone) and silicate (sandstone) aquifers offer the potential for CO_2 storage and sequestration (Law and Bachu, 1996). Injection of CO_2 into formation waters results in chemical reactions that lower the pH, causing the acidic formation water to dissolve the aquifer rock minerals or cement (Emberley et al., 2005; Kharaka et al., 2009). Both carbonate and silicate aquifers react with the injected CO_2. Carbonate aquifers have higher reactivity to dissolve more calcite, while silicate aquifers are more likely to precipitate carbonate minerals (Gunter et al., 2000; Kaszuba et al., 2005).

Aquifer characteristics required for CO_2 storage include depth greater than or equal to 800 m, porosity greater than or equal to 12%, permeability >10 millidarcys (mD) for injectivity, and a confining layer or seal (van der Meer, 1993; Nelms and Burke,

2004). In addition, the aquifer should be located in a stable environment (geological and political) and near the production of CO_2 (Bachu, 2000).

Chemical Reactions

When CO_2 dissolves in water, it forms weak carbonic acid

$$CO_{2\,(g)} + H_2O \leftrightarrow H_2CO_3 \quad (1)$$

which dissolves limestone by the following reaction

$$CaCO_3 + H_2CO_3 \leftrightarrow Ca^{2+} + 2HCO_3^- \quad (2)$$

Under basic pH conditions, bicarbonate further dissociates to

$$HCO_3^- \leftrightarrow CO_3^{2-} + H^+ \quad (3)$$

resulting in carbonate ions in solution. When the water is a NaCl solution, the salt dissociates into sodium and chloride ions

$$CaCO_3 + H_2O + CO_2 + NaCl \leftrightarrow Ca^{2+} + 2HCO_3^- + Na^+ + Cl^- \quad (4)$$

Several experimental studies of water-rock-CO_2 reactions under geologic conditions verified the presence of acidic solutions resulting in the dissolution of limestone (Gunter et al., 2000; Kaszuba et al., 2005; Gledhill and Morse, 2006; Finneran and Morse, 2009; Ketzer et al., 2009). Gunter et al. (2000) and Emberley et al. (2005) found dissolution of limestone takes place rapidly with calcium and carbonate ions increasing in solution early during CO_2 flooding. Carbonate aquifers are not good for mineral trapping due to the excess calcium and carbonate ions in solution. Carbonate in solution reacts with divalent cations dissolved from the host rock or in the brine for mineral precipitation (Xu et al., 2004). Limestone host rocks have few divalent cations, other than calcium, available for mineral precipitation. Dolomites can contribute magnesium ions to increase the potential for new carbonate mineral precipitation.

Some laboratory experiments of CO_2 flooding have shown that CO_2 reacts with the brine and carbonate rock to form preferential dissolution channels (Grigg et al., 2005; Izgec et al., 2008). The preferential dissolution increases porosity and permeability of the rock along the flow path of injected CO_2.

Geology and Hydrogeology of the Madison Group in the Williston Basin

The Williston Basin is a large, structurally simple, tectonically stable, sedimentary basin located entirely within the North American Craton. It covers 500,000 square kilometers, including parts of Montana, Saskatchewan, Manitoba, and most of North Dakota, with the deepest part of the basin centered near Williston, North Dakota. The Williston Basin contains a nearly complete stratigraphic record from the Cambrian to the Tertiary (Figure 1), with sediment deposition over 4500 m thick (Gerhard et al., 1982). While the basin is considered structurally simple, it does contain some anticlines, synclines, and near vertical faults (Fischer et al., 2005a). The stratigraphy is well understood as a result of oil and gas exploration. Figure 1 shows the stratigraphic column from the Cambrian through the Quaternary for the Williston Basin in North Dakota with the principal aquifers (AQ) and confining units (TK) as defined by Downey (1984, 1986). A designation of TK does not necessarily imply that all formations and layers within that unit are aquitards, but rather, the unit as a whole behaves as an aquitard. Several TK units contain smaller aquifers within the layers, and several AQ units contain aquitards within the layers. These unit designations are helpful to recognize potential sequestration units within the Williston Basin.

The Madison Group is the primary oil-producing unit in the Williston Basin and is under consideration for CO_2 sequestration in saline aquifers and/or as a target for EOR

Age Units			YBP (Ma)	Rock Units		Hydrologic Systems
Phanerozoic	Cenozoic	Quaternary	1.8			AQ5 Aquifer
		Tertiary		White River Grp		
				Golden Valley Fm		
			66.5	Fort Union Grp		
	Mesozoic	Cretaceous		Hell Creek Fm		
				Fox Hills Fm		
				Pierre Fm		TK4 Aquitard
				Niobrara Fm	Colorado Group	
				Carlile Fm		
				Greenhorn Fm		
				Belle Fourche Fm		
				Mowry Fm	Dakota Group	AQ4 Aquifer
				Newcastle Fm		
				Skull Creek Fm		
			146	Inyan Kara Fm		
		Jurassic		Swift Fm		TK3 Aquitard
				Rierdon Fm		
			200	Piper Fm		
		Triassic	251	Spearfish Fm		
	Paleozoic	Permian		Minnekahta Fm		
				Opeche Fm		
			299	Broom Creek Fm	Minnelusa Group	
		Pennsylvanian		Amsden Fm		AQ3 Aquifer
			318	Tyler Fm		
		Mississippian		Otter Fm		TK2 Aquitard
				Kibbey Fm		
				Charles Fm	Madison Group	
				Mission Canyon Fm		AQ2 Aquifer
				Lodgepole Fm		
			359	Bakken Fm		TK1 Aquitard
		Devonian		Three Forks Fm		
				Birdbear Fm		
				Duperow Fm		
				Souris River Fm		
				Dawson Bay Fm		
				Prairie Fm		
				Winnipegosis Fm		
			416	Ashern Fm		
		Silurian		Interlake Fm		
			444	Stonewall Fm		AQ1 Aquifer
		Ordovician		Stony Mountain Fm		
				Red River Fm		
				Winnipeg Grp		
			488	Deadwood Fm		
		Cambrian	542			

Figure 1. Modified stratigraphic column of the Williston Basin in North Dakota. After Downey, 1984; Bluemle et al., 1986; Fischer et al., 2005c.

operations (Jiang, 2002; Fischer et al., 2005a, 2005b, 2005c). The Madison Group contains the Lodgepole, Mission Canyon, and Charles Formations, which were deposited during the Mississippian (Heck, 1979; Fischer et al., 2005a). The Lodgepole and Mission Canyon Formations are carbonates and together form aquifer group AQ2 (Downey, 1984). The Lodgepole overlies the Bakken Formation, an oil-producing shale unit that acts as an aquitard (included in TK1). The Lodgepole limestone is believed to be the source of some of the Madison oil (Jiang, 2002). The Charles Formation is an evaporite deposit that acts as a confining layer, TK2, over the Mission Canyon Formation (Downey, 1984). The Mission Canyon contact is conformable with both the Lodgepole and Charles Formations except along the eastern margin of the basin (Heck, 1979). The depth to the top of the Madison group is approximately 2286 m (Nelms and Burke, 2004; Zhou et al., 2008b), deeper than the required 800 m for CO_2 storage. The Madison Group carbonates have an average porosity of 9-13% and evaporites of the Charles Formation provide a competent top seal (Fischer et al., 2005b), conditions favorable for CO_2 storage.

The Williston Basin contains several salt layers, the thickest being the Devonian Prairie Formation with a maximum thickness over 192 m (LeFever and LeFever, 2005). Salt dissolution has led to the high concentration of TDS in the formation waters, as well as several structures formed from the collapse of rock following the salt dissolution (LeFever and LeFever, 2005). Salt beds approximately 30.5 m thick in the Madison overlie the Madison brine and salt dissolution is the likely origin of the Madison brine (LeFever, 1998). The Madison brine is typically composed of NaCl (Downey and Dinwiddie, 1988). Brine concentrations in the Madison aquifer range from 1,000 ppm

near recharge areas to over 300,000 ppm total dissolved solids (TDS) near the deeper part of the Williston Basin (Downey, 1984; Busby et al., 1995).

Regional flow of formation waters in the Madison Group is to the north-northeast at a rate of approximately two feet per year (Downey, 1984; Downey and Dinwiddie, 1988; Bachu and Hitchon, 1996; LeFever, 1998). The potentiometric surface of the Madison aquifer shows steeper slopes near the recharge areas to the southwest, and is nearly horizontal and hydrostatic near the center of the Williston Basin (LeFever, 1998). Recharge of the Madison aquifer occurs to the southwest near the Black Hills, Beartooth Mountains, and Snowy Mountains, where the rocks crop out at the surface. The Madison aquifer rocks do not crop out to the east, therefore aquifer discharge is a result of vertical leakage (Downey, 1984).

Enhanced Oil Recovery in the Williston Basin

Depleted oil reservoirs that are suitable for EOR by CO_2 are those in advanced stages of water flooding (Holtz et al., 2001). CO_2 enhances oil recovery after primary production and secondary recovery from water flooding by displacing residual oil and miscible mixing to reduce the viscosity (Holt et al., 1995; Hitchon et al., 1999; Qi et al., 2009). Approximately 30% of the CO_2 injected for EOR remains in the reservoir for storage (Gunter et al., 2000); the rest is produced with the oil and re-injected (Hitchon et al., 1999; Qi et al., 2009).

Currently EOR operations inject a minimal amount of CO_2 as needed and the CO_2 remains in the formation for a short duration, on the order of a few years. Desired CO_2 storage in depleted oil reservoirs would involve maximum amounts of CO_2 injected and residence time of thousands of years (USDOE, 2002). CO_2 storage in depleted oil

reservoirs is an attractive option as the infrastructure is already in place in many of the fields (Holt et al., 1995; Fischer et al., 2005a). Figure 2 shows the locations of oil fields in North Dakota. The majority of producing oil fields are located along the Nesson Anticline near the center of the Williston Basin in western North Dakota. The fields highlighted in yellow are oil fields that have produced from some portion of the Madison through early 2009 (LeFever, 2009). These fields may be suitable for CO_2 storage or EOR operations.

A better understanding of geochemical changes resulting from CO_2 flooding is needed before CO_2 sequestration can safely and effectively take place in depleted oil fields as part of EOR or storage in saline aquifers in the Williston Basin in North Dakota.

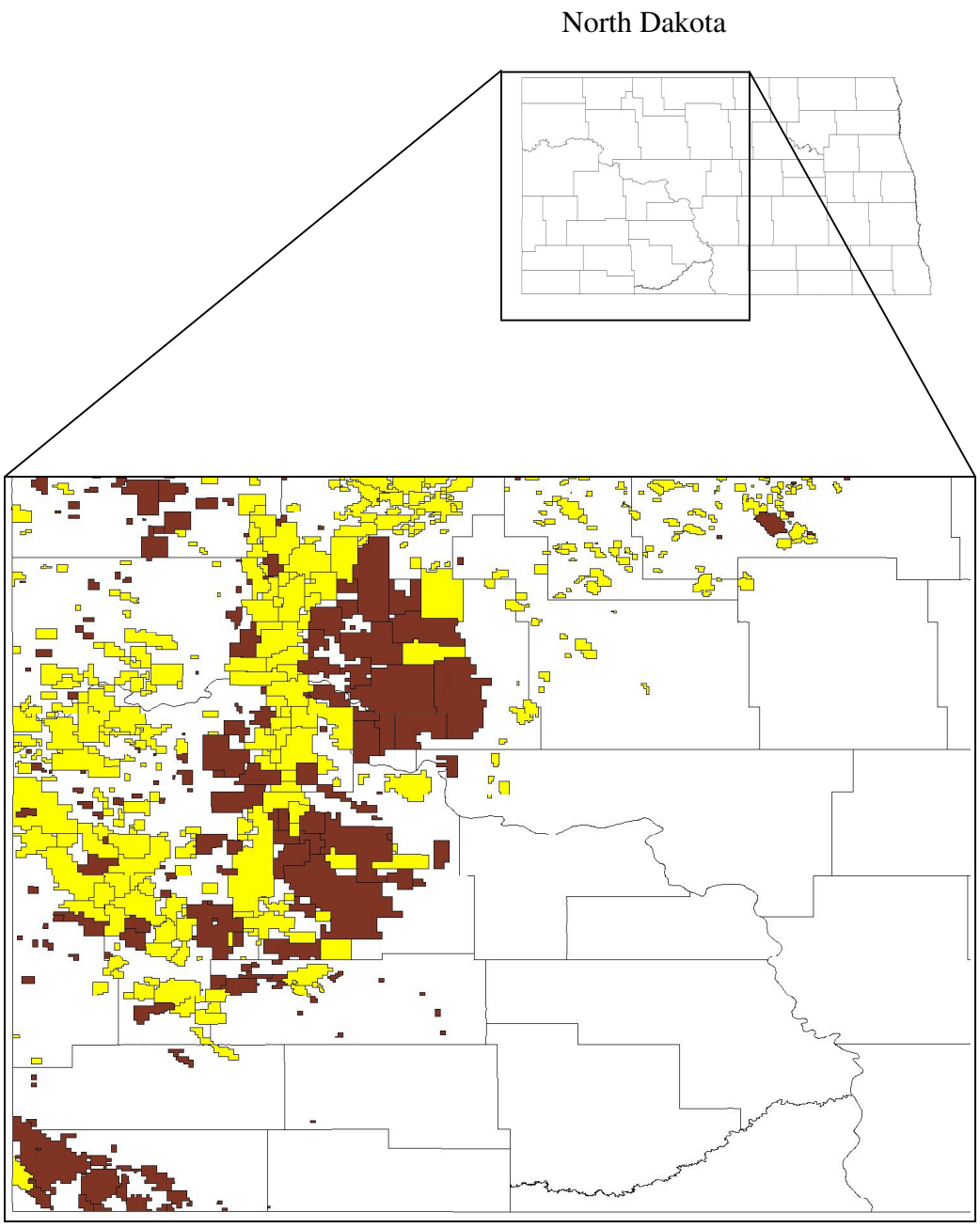

Figure 2. Oil fields in North Dakota. Fields highlighted in yellow are Madison Group fields. Map courtesy of North Dakota Department of Mineral Resources Oil and Gas Division GIS.

CHAPTER III

MATERIALS AND METHODS

Core Flooding System and Experimental Procedures

Core flooding experiments were conducted in January and February 2009, using a core flooding system developed by Zeng (2006) in the Petroleum Engineering Laboratory at the UND Geology and Geological Engineering Department (Figure 3, Appendix A). The core flooding system simulates the carbon dioxide (CO_2) injection process at subsurface conditions with the capacity to regulate in-situ stresses, pore fluid pressure and temperature exerted on the rock and fluid. Pumps alternately or concurrently inject supercritical CO_2 and saline water or other fluids. The entire system is controlled and monitored using a computer. The axial and radial stresses, fluid pressures at the inlet and outlet, temperature, and fluid volume in the pump are recorded continuously.

A prepared rock core is placed in the core chamber, which is then sealed. The core chamber assembly is enclosed in an oven programmed to maintain a constant temperature. Axial and radial stresses are applied and pore pressure is regulated. In these experiments, axial and radial pressures were both set to 32.8 MPa, simulating overburden insitu stress. Pore pressure was held between 17.2 –18.6 MPa using a back-pressure regulator (BPR). The oven temperature was maintained between 57-60°C. An in-line filter was used in place of BPR1 (Figure 3) to prevent particles in the injection fluids from clogging the pores of the rock.

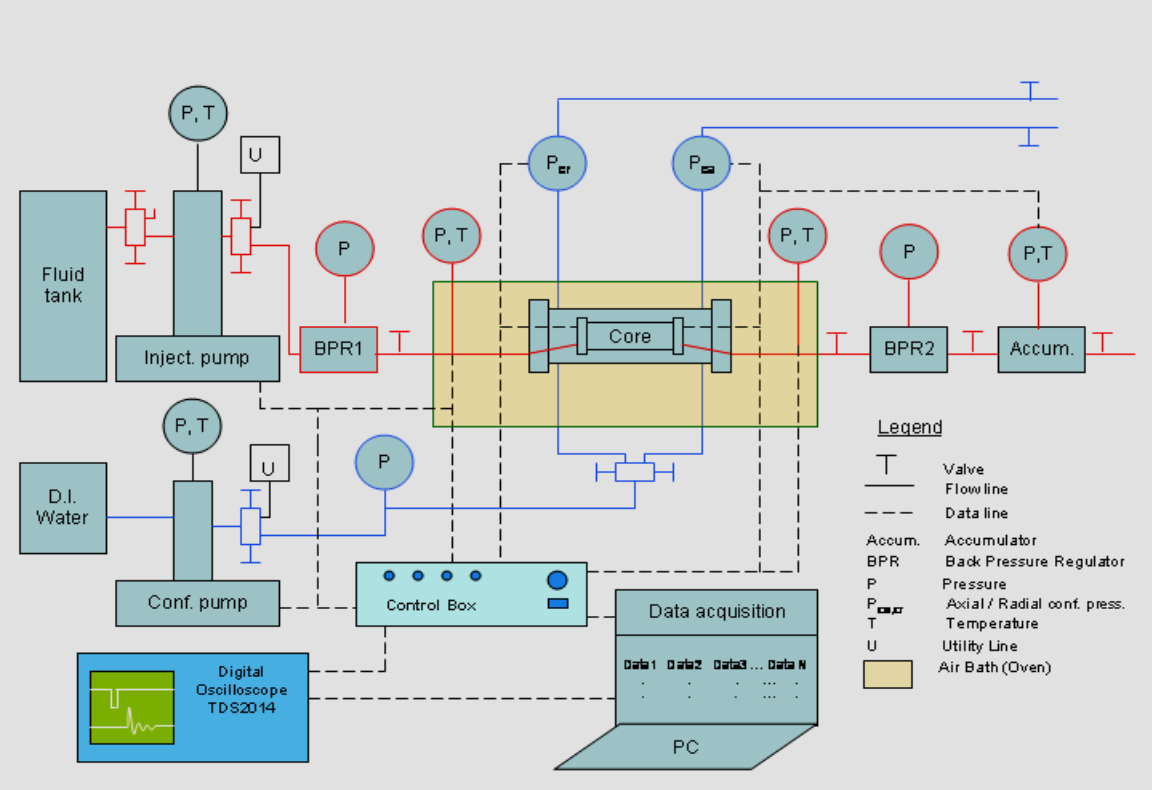

Figure 3. Multipurpose core flooding system. After Zeng, 2006.

The temperature and pressure selected for these experiments are similar to conditions that may be encountered under enhanced oil recovery (EOR) operations in the Madison Group oil fields of Williston Basin. The temperature and pressure values were also selected to remain consistent with other research concurrently taking place utilizing this system.

Once the temperature and pressure have stabilized, flooding can begin. ISCO syringe pumps were used to control the pressure and flow rate of fluids through the system. Water-alternating-gas (WAG) flooding was conducted at a volumetric rate of 1:2 V_{CO2}:V_{H2O}, starting with CO_2, followed by water (H_2O). One WAG cycle consists of 200 ml of CO_2 and 400 ml of H_2O and takes approximately 24 hours to complete. Each experimental run consists of five WAG cycles, which take approximately 5 days to

complete, for a total of 3000 ml of injected CO_2 and H_2O. Based on initial pore volumes, each cycle represents approximately 50 pore volumes of CO_2 and 100 pore volumes of H_2O injected (Appendix B). A computer continuously recorded the date, time, temperature, pressure, pump fluid volume, and flow rate data throughout each experiment. The data was recorded on average, of every six seconds.

Supercritical CO_2 flooded the core at a constant rate of 0.5 ml/min. The CO_2 effluent was discharged into a plastic container containing 500 ml of DI water, initially, and is released in pulses as the CO_2 escapes the BPR. Specific conductance (conductance) and pH of the effluent solution were measured and recorded approximately every hour.

Following the CO_2 flood, saline water was injected through the system at a rate of 0.43 ml/min. The effluent of each saline water cycle was collected in a glass jar for laboratory analysis, along with pH and conductance measurements recorded hourly. The saline effluent was constantly mixed with a magnetic stir bar and stir plate. At the end of each water flood, the effluent sample was mixed and placed in separate plastic bottles with appropriate preservatives for the analyses.

The injection pump was rinsed with DI water following each cycle of saline water flooding (Appendix B), resulting in down-time for the system and required correction of recorded data. The pump was thoroughly flushed at the conclusion of the 100,000 ppm experimental run.

Rock Core Preparation

Cylindrical rock cores were prepared from a block of quarried Indiana Limestone, also known as Salem Limestone (Appendix A). Indiana Limestone is used as a reference

for carbonate reservoir rocks for CO_2 sequestration because many of its properties are similar to carbonate reservoir rocks that may be used for CO_2 sequestration or enhanced oil recovery. Indiana Limestone is a bioclastic calcarenite of Mississippian age. It is composed mainly of sand sized bryozoan and echinoderm fossil fragments less than 1 mm in length, uniform in grain size and bound together with a calcite matrix likely derived from carbonate mud (Smith, 1966). The Indiana limestone is about 98 wt % $CaCO_3$ with trace amounts (<0.5 wt %) of SiO_2, Fe_2O_3, MgO, Na_2O and K_2O (McGee, 1989).

Each core has a diameter of 2.54 cm, height of 5.08 cm and a mass of approximately 50 g. Physical properties of the cores were measured pre- and post-CO_2 flooding and geomechanical testing (Appendix B).

Saline Solution Preparation

Four WAG experiments were conducted, each with saline water at different levels of salinity. NaCl solutions were prepared at levels that may be encountered in the aquifers of the Williston Basin, including 1,000 ppm, 10,000 ppm, and 100,000 ppm NaCl solutions. All NaCl solutions will be referred to as saline solutions. A reference test using DI water was performed to create a baseline of data. For comparison purposes, seawater has a salinity of about 35,000 ppm.

Four liters of saline solution were needed for each experimental run. The saline solutions were prepared in the UND Environmental Analytical Research Laboratory (EARL) in Leonard Hall using laboratory grade NaCl (Table 1, Appendix A).

Table 1. Stock Solution Preparation

Stock Solution	Desired Concentration (ppm)	Mass of NaCl (g)	Solution Volume (l)	Calculated Concentration (ppm)	Calculated Concentration (M)
A	10,000	20.0040	2	10,000.5	0.17
		19.9962	2		
B	1,000	2.0014	2	1,000.15	0.017
		1.9992	2		
C	100,000	200.0048	2	99,993.5	1.7
		199.9693	2		
D	0	0.0000	4	0	0

Sample Collection

After 400 ml of saline water flood have passed through the system, the water sample was collected, mixed, and stored in separate plastic bottles for later analysis. Cations were preserved with 2 ml concentrated nitric acid; anions, TDS and alkalinity were not acidified. All samples were labeled and stored in the refrigerator at 4°C. Five water samples representing the five cycles of flooding were collected for analysis. Due to the experimental design and volume required for laboratory analysis, sample frequency was limited to one sample per WAG cycle. The water effluent samples and measurements are referred to as water flood samples. Sample IDs begin with a letter (A = 10,000 ppm, B = 1,000 ppm, C = 100,000 ppm, and D = 0 ppm) followed by a number, 1-5, representing the cycle number. For example, sample A3 refers to the third cycle of the 10,000 ppm water flood. Descriptions of the sample IDs are located in Appendix B.

The DI water used to collect CO_2 effluent was also collected for a sample. The water was used to bubble CO_2 throughout all five WAG cycles, thus this sample

represents the accumulation of ions over the entire duration of each experiment. Due to degassing of CO_2, a chemical imbalance led to the rejection of the data.

Laboratory Analysis

Aqueous samples for laboratory analysis were analyzed in the UND Environmental Analytical Research Laboratory (EARL) in Leonard Hall. Sodium, calcium, iron, and magnesium were analyzed by flame atomic absorption spectroscopy (FAAS). Chloride was measured on an ion chromatograph (IC). Total dissolved solids (TDS) were measured following the procedure by Hem (1985). Alkalinity was determined by Hach (2007) colorometric titration. Detailed methodologies are presented in Appendix A.

Calcium calibration standards were prepared using a volume of NaCl solution that contained a similar concentration of sodium ions in solution as the samples being analyzed. NaCl was added to the calcium calibration standards for the 10,000 ppm and 100,000 ppm solutions in order to strengthen the calcium results by having a similar matrix as the standards.

Several samples required dilutions in order for the measured concentration to fall within calibration standards (Appendix B). Dilutions were prepared using Equation (5)

$$C_1V_1 = C_2V_2 \quad (5)$$

Where C is the concentrations and V is the volume. The dilution factor (DF) is calculated using Equation (6)

$$DF = V_2/V_1 \quad (6)$$

Quality assurance (QA) duplicate analyses were conducted at a rate of 10% while matrix spike analyses were conducted at a rate of 20%. Duplicate analyses were evaluated using Equation 7

$$\% \text{ Difference} = \left(\frac{C_1 - C_2}{C_1 + C_2}\right) \times 100 \quad (7)$$

When the result of Equation (7) was less than 10%, the values were determined to be reproducible. If the result of Equation (7) was greater than 10%, the sample was re-tested rather than rejected due to the limited number of samples collected. Samples were re-tested by preparing new dilutions from the original sample and re-analyzed.

Spike recovery analyses were evaluated using Equation (8)

$$\% \text{ Recovery} = \left(\frac{C_3V_3 - C_1V_1}{C_2V_2}\right) \times 100 \quad (8)$$

where the difference between the spiked solution values (3) and the original sample values (1) are divided by the standard spiking solution values (2). When the result of Equation (8) was between 80% and 120%, the values were determined to be accurate. If the result of equation (8) was outside the window, the value was re-tested rather than rejected due to the limited number of samples collected. In some cases, sodium water was added to the calibration standards for more accurate measurements and all samples were re-tested. High levels of sodium easily mask calcium; therefore several calcium samples were analyzed with sodium in the standards. Quality control data is presented in Appendix B.

CHAPTER IV

RESULTS

Water-Alternating-Gas Flooding

Core flooding was completed for four different saline water concentrations. The pressure and temperature were held at the appropriate levels for all but the 100,000 ppm flood. During the last cycle of the 100,000 ppm flood, the computer system stopped working, likely the consequence of corrosion in the system from the high salinity. All results for Cycle 5 of the 100,000 ppm flood must be considered as estimates. After the computer system stopped working, it was unknown if the core flooding system retained the appropriate pressures and temperature. Core flooding continued until fluid of Cycle 5 was completely injected through the system.

Physical Properties of Rock Cores

Following WAG flooding, the cores underwent geomechanical testing as part of other research conducted concurrently with the saline water floods. Stresses applied to the rock cores post-flooding often resulted in fracturing of the rock, therefore changes to the physical characteristics of the rock must be considered as estimates. It is unknown the extent of changes attributable to WAG flooding versus geomechanical testing. Results of the changes in porosity and density are listed in Table 2. Detailed calculations are available in Appendix B.

Table 2: Flooding induced changes in porosity and density of rock cores. Conc – Concentration, φ – porosity, ρ – bulk density, g/cm^3.

Specimen	Conc. (ppm)	φ_0	φ_1	$\Delta\varphi$	$\Delta\varphi$ %	ρ_0	ρ_1	$\Delta\rho$	$\Delta\rho$ %
08IL115	0	0.150	0.162	0.012	8.22	2.34	2.15	-0.20	8.50
08IL116	1,000	0.161	0.161	0.000	0.00	2.35	2.14	-0.21	8.93
08IL106	10,000	0.156	0.159	0.002	1.32	2.36	2.14	-0.22	9.25
08IL114	100,000	0.157	0.165	0.008	5.26	2.36	2.13	-0.23	9.69
				Average	3.70			Average	9.09

Initial porosities, φ_0, (primary porosities) were approximately 0.15-0.16, or 15-16%. Final porosities, φ_1, were approximately 0.16, or 16%. Some of these changes in porosity may be attributed to rock fracturing during geomechanical testing (secondary porosity). All porosities increased following water flooding with the exception of the 1,000 ppm flood, which remained constant. Porosities increased an average of 3.70% over the initial porosity following flooding and geomechanical testing. The DI water flood had the largest increase of 8.22%.

Initial densities were approximately 2.35 g/cm^3, on the low end of typical mineral densities. Calcite has an average density of 2.71 g/cm^3, however, these cores likely have higher porosities due to the fossiliferous component of the structure. Average change in density post flooding was a 9% decrease. Increased porosity and decreased density suggest the mineral structure is dissolving during flooding and the dissolved species are flushed out of the system, rather than precipitating as new minerals.

Effluent pH

Effluent pH measurements indicate a sharp contrast between CO_2 flooding and saline water flooding. Generally, pH readings were moderately acidic during CO_2 flooding and slightly acidic during saline water flooding. Figure 4 shows the pH during

all four flooding experiments. A table showing the pH values used to create the graph appears in Appendix B.

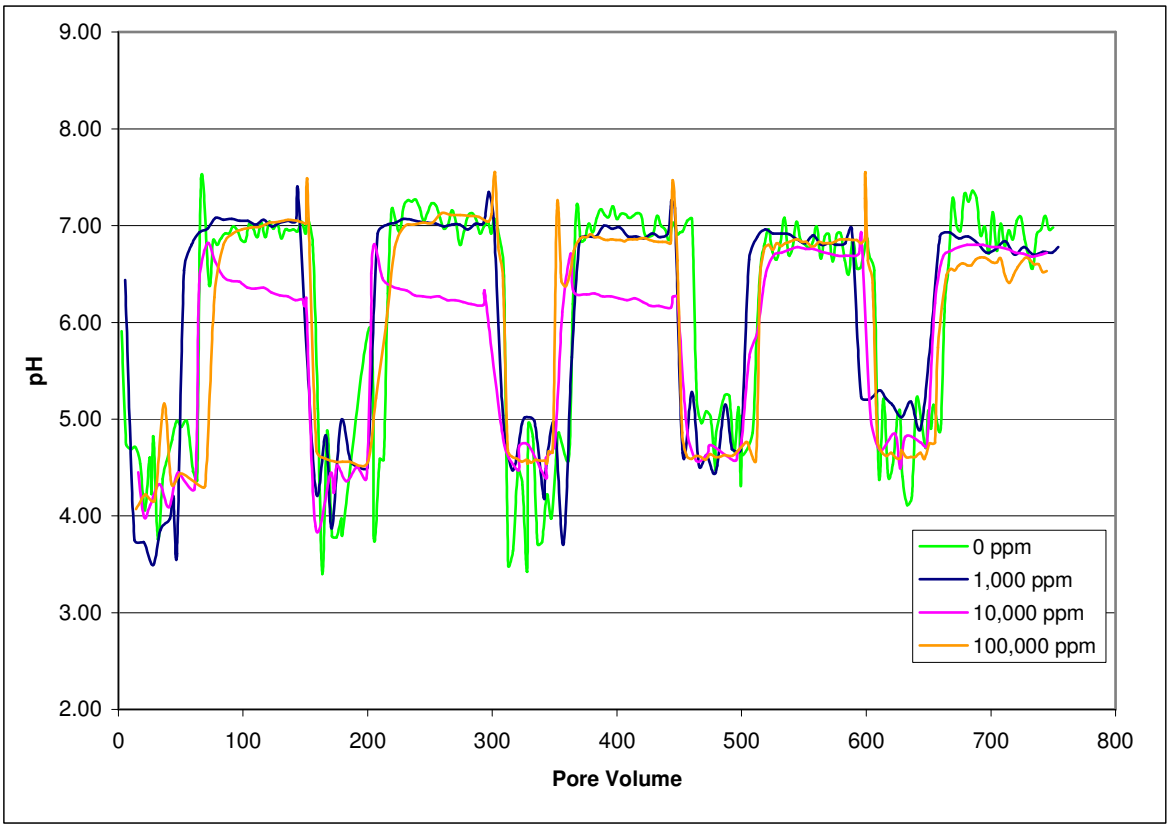

Figure 4. Effluent pH during flooding.

CO_2 flooding causes abrupt changes to pH upon discharge to the effluent container. CO_2 rapidly de-gasses and escapes to the atmosphere when it flows out of BPR2. Thus, the pH measured in the effluent is not representative of the pH of the solution at geologic conditions. At best, the pH data can be viewed as trends, but not accurate values. The variation in pH under CO_2 flooding is likely due to poor mixing of the effluent upon CO_2 discharge.

It is well known that CO_2 dissolves in water to form a weak acid; therefore, it is likely pH is even lower inside the core flooding system than was measured in the

effluent. The pH measurements collected during these experiments verify a decrease in pH when CO_2 is injected into brine.

Effluent Conductance

Conductance values followed a similar trend as pH, with lower conductance during the CO_2 flood and higher conductance during the saline water flood. Conductance values are proportional to the amount of total dissolved solids in the saline water flood (Hem, 1985). Figure 5 shows the conductance during all four saline flooding experiments. A table showing the conductance values used to create the graph appears in Appendix B.

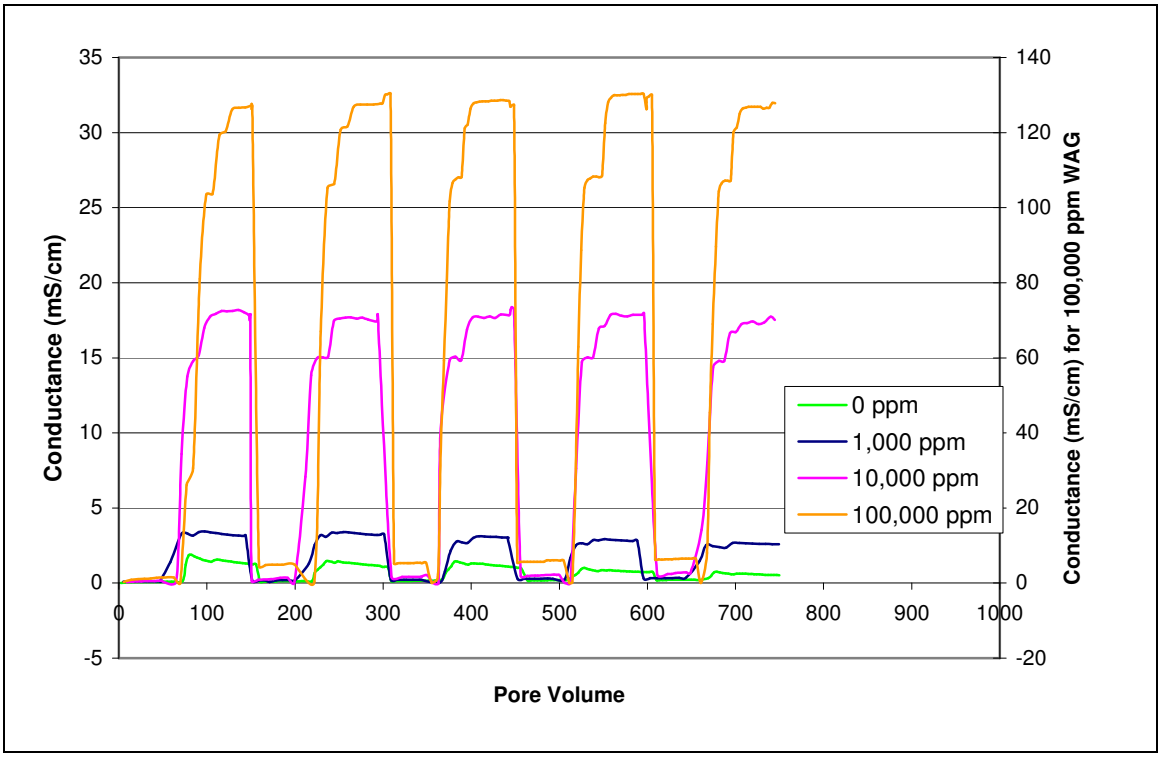

Figure 5. Effluent conductance during flooding.

during the first cycle of DI water flood shows the largest value of conductance, 1.87 mS/cm, at the initial water flood breakthrough. Conductance has an initial peak at water flood breakthrough then generally decreases throughout each successive water flood

cycle. Each water flood cycle has a lower peak conductance value than the previous cycle. This suggests that the chemical reactions taking place between the rock, water and CO_2 occur rapidly, with the water flood flushing out the dissolved ions from limestone dissolution. Conductance values during DI water flooding should be near zero unless dissolution is taking place, releasing ions into solution.

Conductance values for 1,000 ppm, 10,000 ppm, and 100,000 ppm all follow similar trends, with conductance of the CO_2 flood near zero and the conductance for the water flood elevated proportional to the salinity. Additional conductance resulting from dissolution during the saline flooding is likely masked due to the high TDS in the solutions. Peak conductance values are around 3.4 mS/cm, 18 mS/cm, and 138 mS/cm for the 1,000 ppm, 10,000 ppm, and 100,000 ppm water floods, respectively.

Chemical Analysis

Laboratory analytical results are presented in Table 3. Detailed methodologies are located in Appendix A.

An ion balance was computed on the data and several of the ion balances were not within an acceptable range, suggesting the presence of ions in solution that were not analyzed, masking effects by the high NaCl concentrations, and/or inaccurate alkalinity measurements. Magnesium, a divalent cation, was analyzed in three samples and determined at low concentrations in those samples. The presence of magnesium did improve the ion balance, however, the concentrations were <0.25% of the total dissolved ions. Therefore, magnesium analysis was not performed on the rest of the samples.

Based on Ca^{2+}, and to a lesser extent alkalinity, the core flooding experiments appear to approach equilibrium by the final cycle, or approximately 750 pore volumes of

injected fluids. Chemical equilibrium was not achieved during the short durations of flooding of each experiment.

Table 3. Results from chemical analyses. All results are reported in mg/l. Na^+ – sodium, Ca^{2+} – calcium, Fe^{2+} – ferrous iron, Cl^- – chloride, HCO_3^- – bicarbonate alkalinity as $CaCO_3$, TDS – total dissolved solids, ^{J} – result is estimated.

Sample ID	Na^+	Ca^{2+}	Fe^{2+}	Cl^-	HCO_3^-	TDS
A	3,731.07	0.29	<0.1	5,778.86	1.4 J	9,987
A1	3,383.24	358.15	0.21	5,866.86	890 J	10,786
A2	3,708.93	343.19	0.24	5,845.06	865 J	10,518
A3	3,703.88	265.85	0.35	5,966.83	920 J	10,442
A4	3,446.91	146.77	0.24	5,937.83	400 J	10,280
A5	3,379.25	127.41	0.11	5,950.65	585 J	10,097
B	374.03	0.59	<0.1	565.36	1.4 J	975
B1	367.15	244.98	<0.1	558.87	730 J	1,685
B2	371.36	241.77	<0.1	568.29	660 J	1,692
B3	315.90	211.61	<0.1	565.13	560 J	1,557
B4	372.90	157.05	<0.1	574.87	425 J	1,434
B5	345.44	119.46	<0.1	576.83	565 J	1,331
C	38,756.26	0.28	<0.1	61,153.55	4.2 J	98,237
C1	36,416.55	428.72	7.05	57,161.13	1,265 J	96,745
C2	37,506.33	375.30	10.09	58,381.14	945 J	97,766
C3	37,759.01	286.96	10.02	59,456.96	975 J	98,271
C4	38,370.26	135.08	1.70	60,308.84	310 J	98,408
C5	37,021.30 J	105.21 J	1.56 J	59,307.50 J	520 J	97,196 J
D	0.20	<0.2	<0.1	4.38	0.8 J	65
D1	1.83	216.70	<0.1	21.49	775 J	758
D2	1.06	198.84	<0.1	11.42	555 J	608
D3	0.77	175.72	<0.1	9.95	765 J	624
D4	0.62	115.94	<0.1	9.17	565 J	395
D5	1.06	90.21	<0.1	9.55	540 J	338

Sodium

Sodium levels remained fairly constant throughout all five WAG cycles. Figure 6 shows the trend of the sodium samples for all experiments. The measured concentrations are close to their predicted concentrations from dissociation, suggesting that sodium is a passive reagent that does not combine to form new minerals, nor is it dissolving from the limestone rock core. All samples, with the exception of the 0 ppm samples, had to be

diluted by several-fold, resulting in an increasing potential for error, which may explain some of the fluctuations in sodium concentrations.

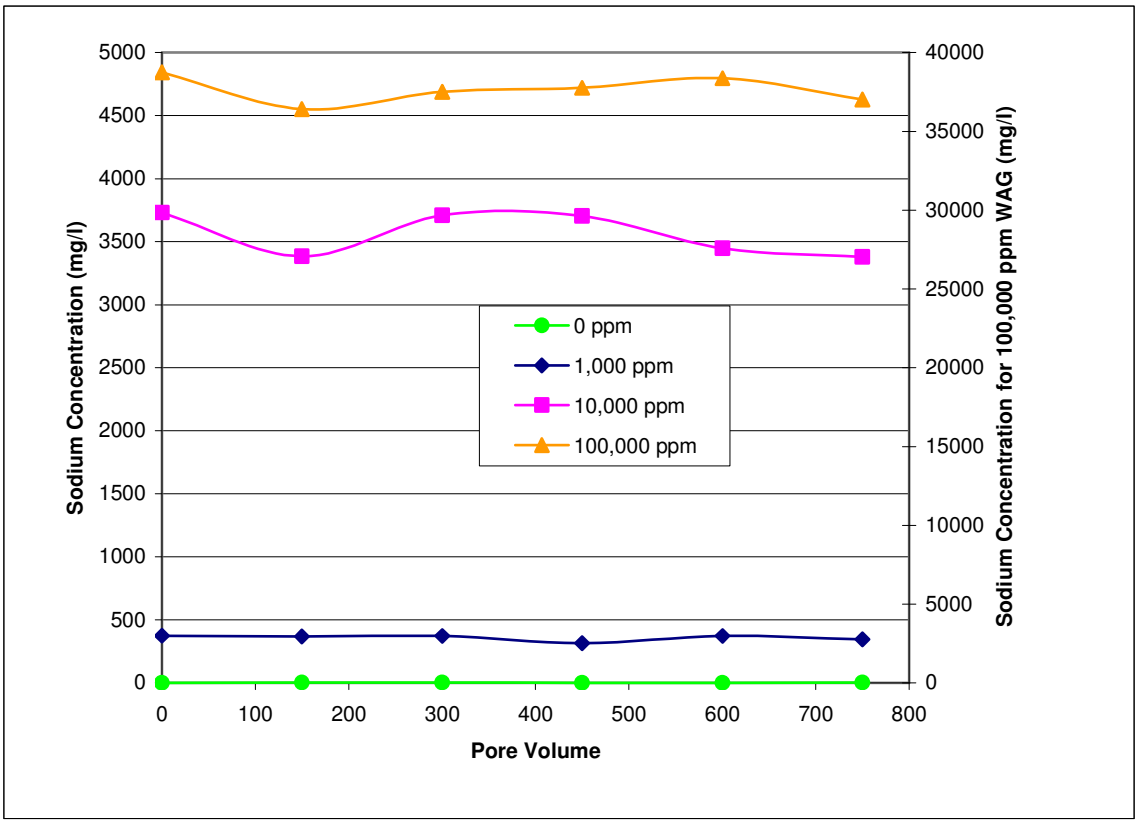

Figure 6. Sodium concentrations for all water flood samples.

Calcium

Calcium concentrations in all of the experiments had a sharp increase after the first water flood with decreasing values through the rest of the cycles (Figure 7). This suggests that limestone dissolution is taking place and that most of the chemical reactions resulting in limestone dissolution occur rapidly. Each level of salinity showed a similar trend, with the DI water flood containing the least amount of dissolved calcium (217 mg/l), followed by the 1,000 ppm and 10,000 ppm floods (245 mg/l and 358 mg/l, respectively). The 100,000 ppm water flood produced the highest amount of dissolved

calcium, at 429 mg/l. The increased calcium concentration with increased salinity suggests that more CO_2 dissolves in water at higher salinity and reacts to form a stronger acid solution than predicted. By Cycle 5, calcium concentrations for all water flooding were between 90-127 mg/l. The data trends appear to be headed toward equilibrium at the end of the experiment, but it would not be known for certain without repeating the experiments for a longer duration.

All samples had to be diluted by several-fold, resulting in an increased potential for error. NaCl was added to the calcium calibration standards for the 10,000 ppm and 100,000 ppm solutions in order to strengthen the calcium results by having a similar matrix as the standards, reducing masking effects by the high concentration of sodium.

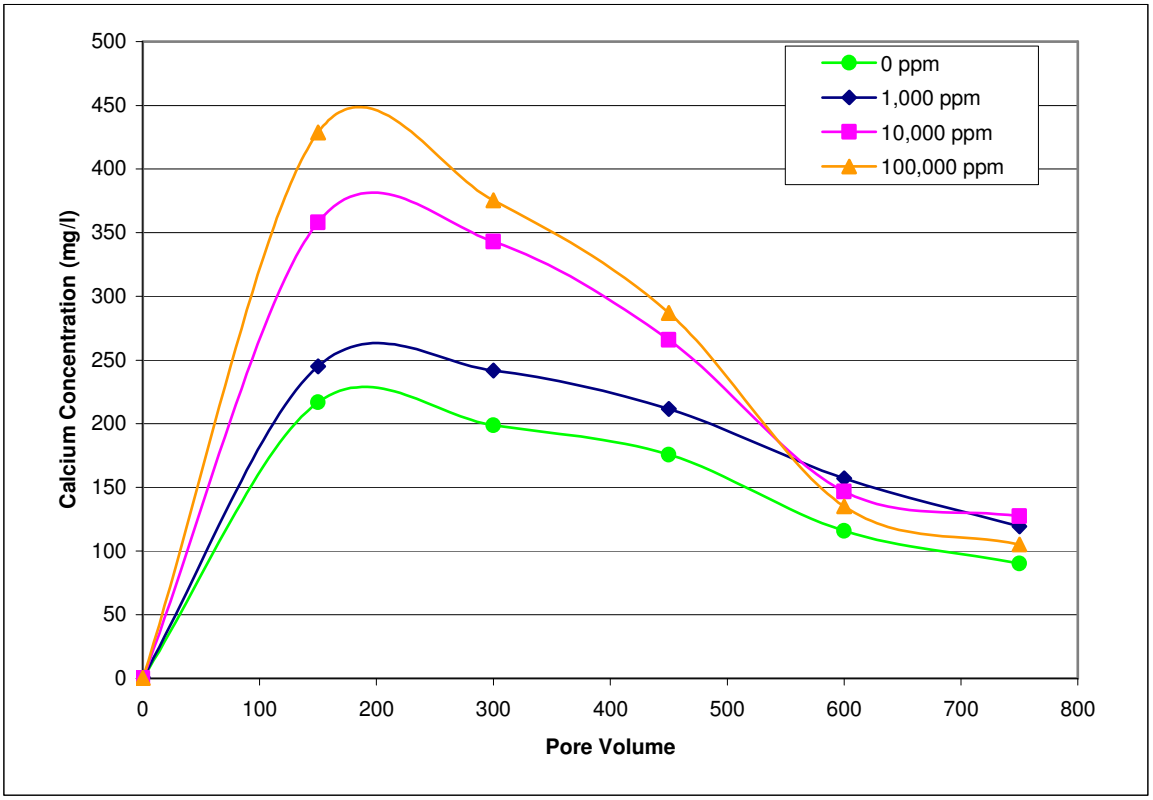

Figure 7. Calcium concentrations for all water flood samples.

Ferrous Iron

Ferrous iron levels were below detection limits for the 0 ppm and 1,000 ppm water floods. Ferrous iron concentrations from the 10,000 ppm flood are less than 0.5 mg/l. Ferrous iron concentrations from the 100,000 ppm flood are between 1.5 and 10.1 mg/l. Figure 8 shows the ferrous iron concentrations from each of the water flood experiments.

Iron in solution could be a result of the dissolution of siderite in the rock core (Testemale et al., 2009). Indiana Limestone is reported as 98 wt % calcite (McGee, 1989), however, it is unknown if siderite is found in the limestone. Iron in solution was most likely a result of corrosion of the system (Hitchon, 2000; Bateman et al., 2005; Gaus et al., 2008).

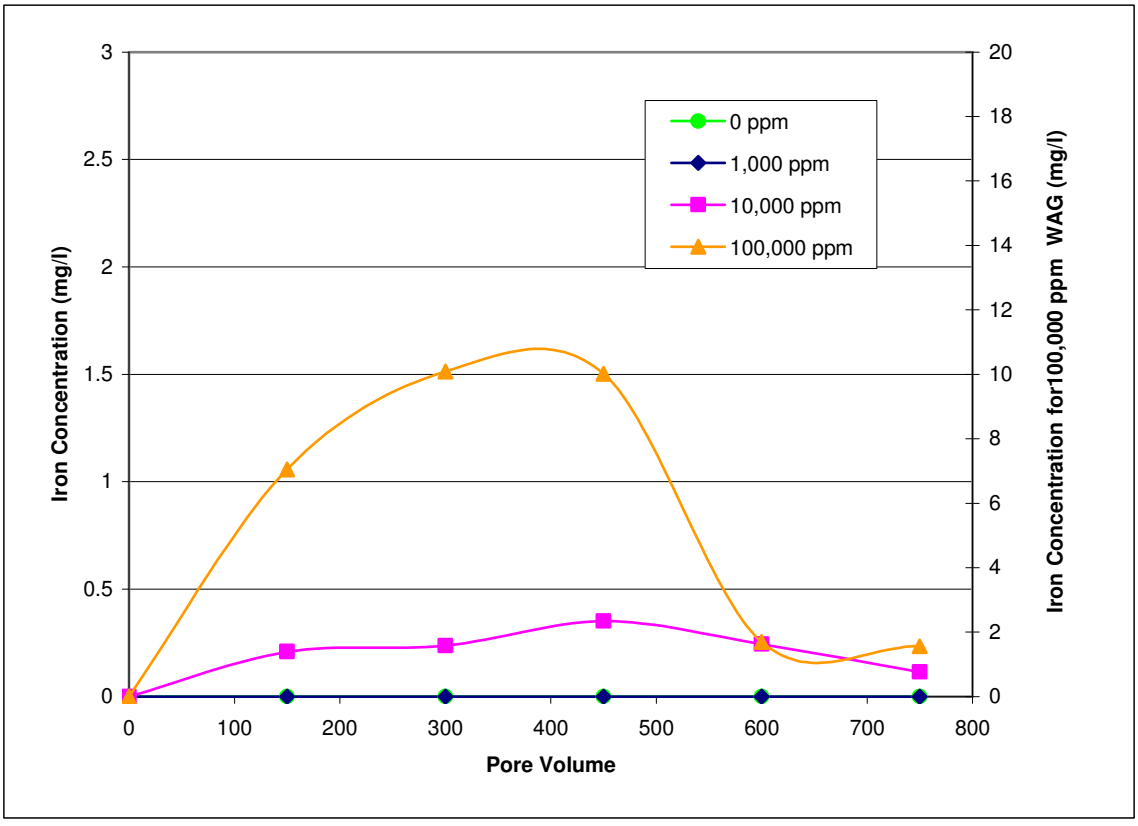

Figure 8. Ferrous iron concentrations for all water flood samples.

Chloride

Chloride levels remained fairly constant throughout all five WAG cycles, similar to sodium. Figure 9 shows the trend of the chloride samples for all experiments. The measured concentrations are close to their predicted concentrations from dissociation. This suggests that chloride is a passive reagent that does not combine to form new minerals, nor is it dissolving from the limestone rock core. All samples, with the exception of the 0 ppm samples, had to be diluted by several-fold, resulting in an increased potential for error, which may explain some of the fluctuations in chloride concentrations.

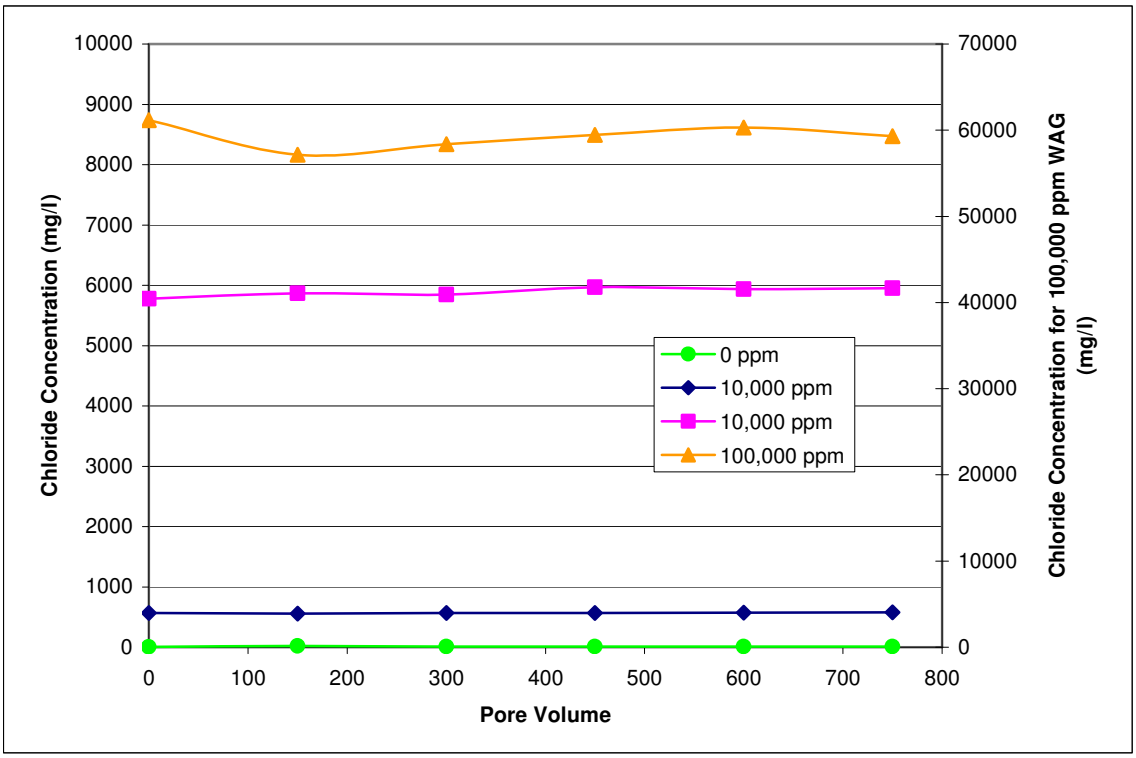

Figure 9. Chloride concentrations for all water flood samples.

Alkalinity

Alkalinity in solution is due to the presence of carbonate, bicarbonate and hydroxide ions in the water. Carbonates are present at high pH, above 8.3. Since the pH was below 8.3 for all samples, no carbonate alkalinity was present in the samples. All alkalinity is bicarbonate alkalinity (Hach, 2007). Figure 10 shows the amount of alkalinity for all WAG experiments. Due to CO_2 degassing, the alkalinity data should only be viewed as trends, not accurate values. Alkalinity values from the effluent are likely lower than alkalinity in the core flooding system due to the escape of CO_2 upon release from BPR 2.

Alkalinity for all samples rose sharply during the first water flood then fluctuated. The 100,000 ppm water flood had the highest alkalinity concentration following the first WAG cycle. Alkalinity acts as a buffer in solution; as more limestone is dissolved, more bicarbonate is released. As more bicarbonate is released, the acidity decreases lessening the amount of limestone dissolved until the solution reaches equilibrium.

Since no carbonates were present in the injection fluid (verified with a titration of the stock solutions), the presence of alkalinity in the water is due to the dissolution of the calcite minerals in the limestone from the reaction of CO_2 and the saline solution.

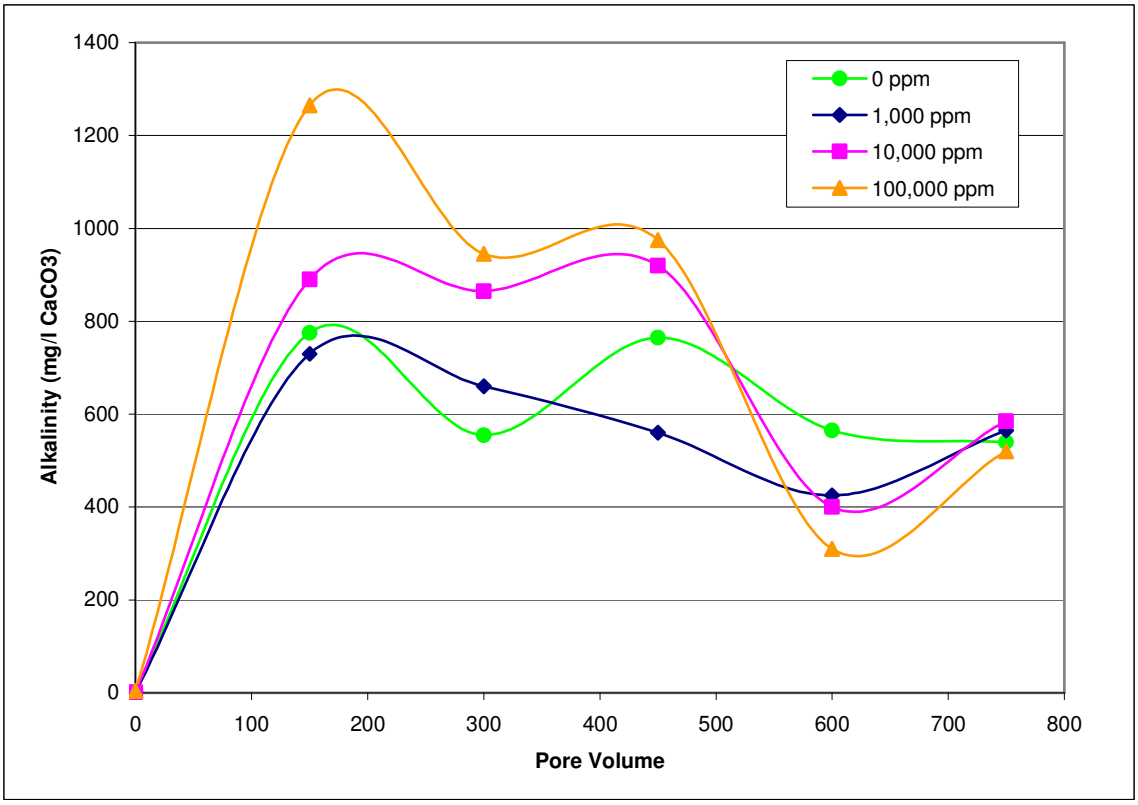

Figure 10. Alkalinity concentrations for all water flood samples.

Total Dissolved Solids

Total dissolved solids (TDS) of all solutions remained fairly constant during the experiment. Figure 11 shows the TDS concentrations throughout the experiments. TDS of all solutions, with the exception of the 100,000 ppm solution, increased after the first water flood. All solutions remained above the initial concentration, indicating dissolution takes place within the rock core. Ions in solution are discharged from the system through the water floods and accumulate in the effluent.

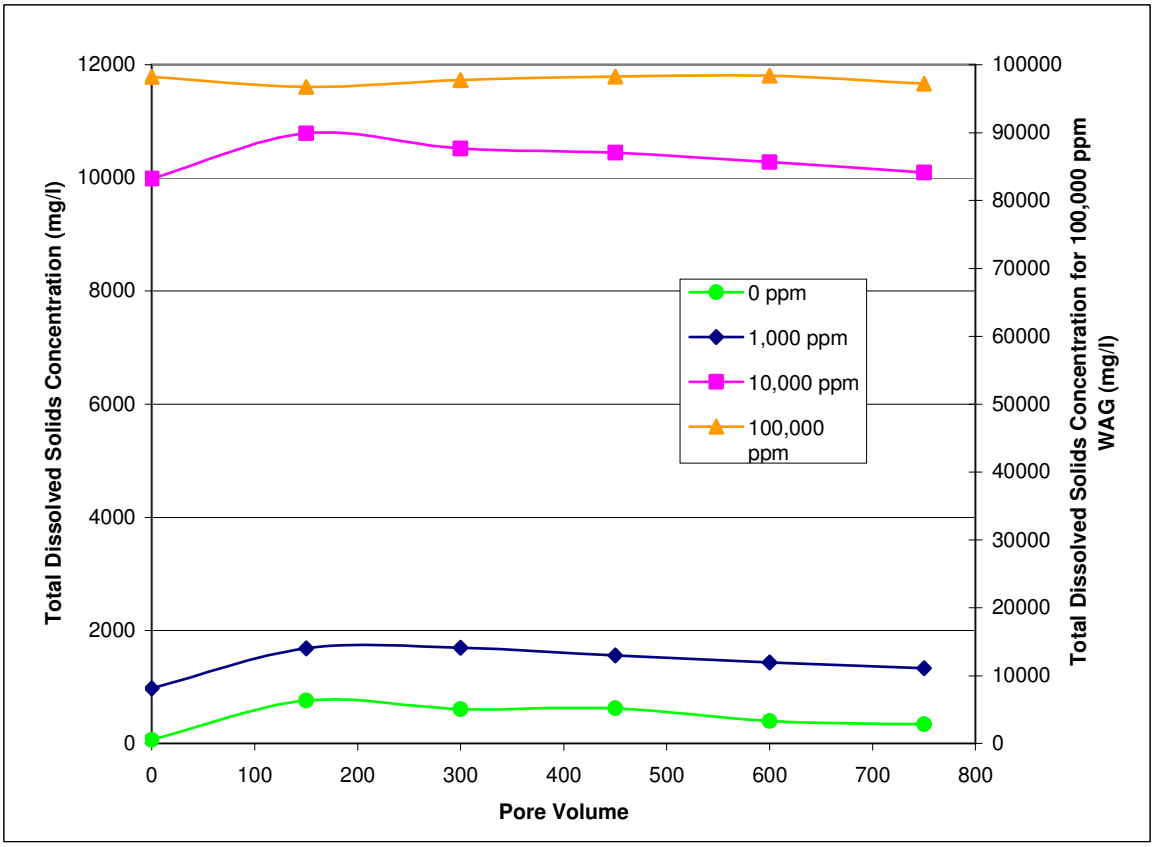

Figure 11. TDS concentrations for all water flood samples.

Water Density

The density of all prepared solutions at standard conditions was determined by pipetting 1 ml of solution onto a balance and recording the mass. The average of 5 aliquots represents the density of the solutions at standard conditions. The density at geologic conditions would be different. Table 4 presents the solution density data. Values used to determine the average density are presented in Appendix B. The density of seawater is listed as a reference. Seawater contains approximately 35,000 ppm TDS.

Table 4. Density of water flood solutions. Density in g/cm^3

Solution	Measured Average density (g/cm^3)	Calculated density >7,000 ppm TDS (g/cm^3)
0 ppm	0.994	-
1000 ppm	0.988	-
10000 ppm	1.001	0.990
100,000 ppm	1.046	1.130
Seawater	1.025	

CHAPTER V

DISCUSSION

Water-alternating-gas (WAG) flooding experiments were conducted on limestone rock cores with deionized (DI) water and three different concentrations of sodium chloride (NaCl) water. The limestone rock cores were composed of at least 98 wt % calcite and had an initial porosity of 15-16%. The average pore volume of each rock core was approximately 3.80 cm^3. NaCl solutions of 1,000 ppm, 10,000 ppm, and 100,000 ppm were selected to represent the lower end of salinity levels found in the Williston Basin. WAG injections are performed to drive CO_2 to move homogeneously, and to reduce the buoyancy of CO_2 by trapping it within the injection fluid and pore space to limit the mobility and potential for escape back to the surface. CO_2 injections are important in the Williston Basin as part of enhanced oil recovery (EOR) programs. Supercritical CO_2 is injected into depleted oil reservoirs where previously immobile oil can be produced, mainly due to miscible mixing with CO_2. The same geologic trap that prevents the escape of hydrocarbons is expected to hold the injected CO_2.

Rock cores were subjected to injection of 200 ml of supercritical CO_2, followed by 400 ml of water solution. Together, these 600 ml represents one WAG cycle; each rock core underwent 5 cycles of WAG flooding for a total of 3,000 ml of injected fluid. Each CO_2 flood pushed approximately 50 pore volumes of CO_2 through the rock core, while approximately 100 pore volumes of saline water were pushed through. CO_2 reacts

with the formation water in the rock to form weak carbonic acid. The acidic solution dissolves the calcite minerals in the limestone, releasing calcium and carbonate ions into solution.

Measured values of effluent pH and conductance show evidence the limestone is dissolving during WAG flooding. During CO_2 flooding, pH is moderately acidic. The CO_2 was discharged to a container of DI water, where the CO_2 escaped to the atmosphere as soon as the pressure was released. Measurements of pH and conductance occurred at standard conditions and may not be an accurate representation of subsurface conditions; pH is likely much more acidic at subsurface conditions. The moderately acidic CO_2 effluent suggests that carbonic acid is forming when CO_2 reacts with the formation water and dissolves the calcite minerals. Water flood conditions increase the pH to slightly acidic. The buffering capacity of carbonates dissolved from limestone may contribute to the higher pH during water flooding. The lower pH during the 10,000 ppm water flood may be a result of poor mixing within the sample. The stir plate was added partway through the 10,000 ppm run to improve sample quality.

Conductance measures the ability of a solution to conduct an electrical current. Generally, the higher the concentration of total dissolved species, the higher the conductance. Each concentration of saline solution and DI water showed minimal conductance and therefore, minimal dissolved ions during the CO_2 flooding. Each concentration of saline solution showed conductance in the anticipated range based on initial salinity. Conductance from DI water flooding would be expected to show minimal amounts of dissolved ions, as DI water contains no initial dissolved ions. However, DI water flood sample conductance shows values up to 2 mS/cm, indicating dissolution

within the rock core is taking place. Dissolution is likely taking place in the other cores during saline water flooding, however, the high initial TDS concentrations of the brines are large enough to mask any dissolution effects.

Sodium and chloride concentrations remain fairly stable through WAG flooding at each level of salinity. This indicates the sodium and chloride ions are not dissolving out of the rock, nor are they precipitating new minerals. The concentrations of sodium and chloride are near the predicated values based on dissociation. Samples for both analyses were diluted by several-fold, which may have resulted in less accurate measured concentrations and account for variations in the concentration throughout the flooding.

Calcium concentrations in all of the water flood samples rose sharply during the first water flood cycle and decreased steadily throughout the rest of the water flood cycles. This suggests that most of the chemical reactions resulting in limestone dissolution occur rapidly, which is consistent with findings by Emberley et al. (2005) and Izgec et al. (2008). The 100,000 ppm water flood Cycle 1 contained approximately 430 mg/l of dissolved calcium, followed by approximately 360 mg/l dissolved calcium in the 10,000 water flood Cycle 1. The 1,000 ppm water flood contained approximately 245 mg/l while the DI water flood contained approximately 220 mg/l. Calcium was absent in the brine, as indicated by the stock solution concentrations; therefore all calcium in solution is a result of limestone dissolution.

CO_2 has been reported as less soluble with higher salinities (Holloway and Savage, 1993; Carr et al., 2003; Izgec et al., 2008), however, the 100,000 ppm water flood had the highest concentration of dissolved calcium and the DI water flood contained the least amount of calcium. This suggests that CO_2 and higher salinity water

react to form a stronger acid solution in geologic conditions than predicted. Each level of salinity showed a similar trend with a large initial increase in calcium followed by a steady decline, which appears to be headed toward equilibrium at the end of the experiment, but it would not be known for certain without repeating the experiments for a longer duration.

Ferrous iron was not on the original analyte list, however, the presence of rust during the 100,000 ppm WAG experiment called into question the amount of iron present in the samples and the source of the iron. Ferrous iron levels were below laboratory detection limits for the 0 ppm and 1,000 ppm water floods. Ferrous iron concentrations from the 10,000 ppm flood are less than 0.5 mg/l. Ferrous iron concentrations from the 100,000 ppm flood are between 1.5 and 10.1 mg/l. The Indiana Limestone is reported as 98 wt % calcite, as such, the iron could result from dissolution of impurities in the limestone.

The combination of high salinity water and CO_2 forms a corrosive liquid that reacts with metals in the system, including the injection tubing and electrodes used to monitor the system via computer. This could have implications for CO_2 injection into saline aquifers for maintaining the integrity of the injection well casing.

The presence of iron in the samples could be a consequence of corrosion of the system, as reported by Hitchon (2000), Bateman et al. (2005), and Gaus et al. (2008). The 100,000 ppm saline water is approximately 3 times greater than the salinity of seawater, so it is expected to find corrosion of metals at such high salinities. Iron was only present in levels above laboratory detection limits in the two highest salinities, confirming CO_2 and brine react to form stronger acids than at lower salinities. It is

impossible to determine from these experiments whether the iron is from corrosion of the system or dissolution of iron minerals in the rock core.

It is also important to note that the computer system shut down during Cycle 5 of the 100,000 ppm flooding. It is unknown if the temperature and pressure remained at the programmed settings during this last cycle. It must be assumed that temperature and pressure did not hold steady and therefore, results from Cycle 5 of the 100,000 ppm WAG flooding must be considered as estimates. It is believed the high TDS concentrations resulted in corrosion of the system and wires connecting the computer electrodes.

Alkalinity measures the ability of water to neutralize acids and is due to the presence of carbonate, bicarbonate and hydroxide ions in the water. Carbonate is present in samples with pH > 8.3. None of the water samples collected exhibited pH > 8.3; therefore, all alkalinity is bicarbonate alkalinity. Alkalinity for all samples rose sharply during the first water flood, again, suggesting the chemical reactions resulting in limestone dissolution take place rapidly upon injection of CO_2 into the system. Water samples collected from each cycle accumulated over a period of several hours, of which the sample was open to the atmosphere. It is probable that some of the carbonate in the water samples converted to CO_2 and carbonic acid, releasing the CO_2 to the atmosphere prior to sampling. Therefore, alkalinity values must be considered as estimates and the data viewed as trends, rather than values. The presence of alkalinity in the samples is due to dissolution of calcite minerals in the limestone, as alkalinity was not present in the stock solutions.

Total dissolved solids (TDS) remained fairly constant throughout all WAG cycles. All solutions from WAG cycles remained above the initial concentration, indicating dissolution takes place within the rock core and ions in solutions are discharged from the system through the water floods, and to a lesser extent, the CO_2 floods. The first WAG cycle showed the largest concentration of TDS for all samples except the 100,000 ppm solution, suggesting most of the limestone dissolution occurs early on in the experiment.

Concentrations for calcium, alkalinity and TDS all increased rapidly during the first cycle, an indication of rapid dissolution of limestone during the early stages of WAG flooding. This coincides with experiments conducted by Emberley et al. (2005) and Izgec et al. (2008), who demonstrated rapid chemical reactions between the brine, rock and CO_2.

Following flooding experiments and geomechanical testing, properties of the rock cores were measured. In all cores except the 1,000 ppm core, porosity increased. The core flooded with DI water showed the largest increase in porosity, over 8%, confirming that CO_2 does react with water and rock to dissolve the host rock. However, the increase in porosity may be a result of fracturing following geomechanical testing of the rock cores. It has been reported that CO_2 is less soluble in more saline solutions (Holloway and Savage, 1993; Carr et al., 2003; Izgec et al., 2008), however, the 100,000 ppm core showed the second highest change in porosity with over 5% increase. The 10,000 ppm core increased porosity over 1%, while the 1,000 ppm core showed no change in porosity. The average increase in porosity was 3.7%. This value is estimated because

some of the porosity may be a result of fracturing of the rock cores during geomechanical testing.

It is important to note that the initial porosities of the rock cores were 0.15-0.16, while the porosity of the Madison Formation in the Williston Basin is 0.09-0.13 (Nelms and Burke, 2004). Caution must be exercised when applying this research to the Madison Group in the Williston Basin, as the difference in porosity could have important implications on CO_2 injectivity and storage. Lower porosities could result in decreased CO_2 injection rates and decreased amounts of CO_2 storage.

Bulk density of each of the cores decreased on average 9%. The core for the 100,000 ppm flood decreased the most, at 9.7%, followed by the 10,000 ppm core at 9.25%, the 1,000 ppm core at 8.9% and the DI core at 8.5%. A decrease in bulk density indicates a loss of solid material, which is another indication of limestone dissolution.

Rosenbauer et al. (2005) conducted a similar experiment using different methods and found a decrease in limestone density of 10% and an increase in porosity of 2.6%. The data collected from these experiments (9% and 3.7%, respectively) are in close agreement with those reported by Rosenbauer et al. (2005).

All rock cores showed a dissolution channel at the entrance where CO_2 was injected into the rock (Figure 12). The 1,000 ppm core showed negligible dissolution upon exit, while the 10,000 ppm core showed slight dissolution upon exit. Experiments conducted by Grigg et al. (2005) and Izgec et al. (2008) also showed a dissolution channel through the rock core. Their rock cores were larger and the duration of their experiment was longer, as such, their cores showed a larger and longer dissolution channel than the cores from these experiments.

These experiments simulating the injection of supercritical CO_2 into a simulated deep, saline aquifer with varying salinities suggest that CO_2 doesn't behave as predicted. Only a few experiments of CO_2 flooding in deep, saline aquifer conditions have been conducted to date. Previous studies and numerical modeling indicate that CO_2 is less soluble with increasing water salinity (Holloway and Savage, 1993; Carr et al., 2003; Izgec et al., 2008). However, more calcium was measured in solution during the 100,000 ppm samples than any other samples from lower salinities during the first three cycles. Samples appear to approach near-equilibrium during the fourth and fifth cycles. Limestone dissolution occurs when CO_2 is dissolved into the formation waters, forming carbonic acid, which reacts with calcite minerals. More ions in solution are an indication of increased limestone dissolution, which is an indication of increased CO_2 solubility in saline waters at geologic conditions.

Two large-scale CO_2 storage projects have shown successful storage of CO_2 in depleted oil reservoirs. The Weyburn Oil Field in Saskatchewan, Canada, has been injecting CO_2 for EOR operations resulting in increased oil recovery and CO_2 storage since 2000 (Preston et al., 2005; Cantucci et al., 2009). Both Preston et al. (2005) and Cantucci et al. (2009) demonstrated the potential for mineral trapping to occur within the carbonate reservoir via numerical modeling.

Portier and Rochelle (2005) conducted numerical modeling of the solubility of CO_2 in saline water at pressures and depths found in the Sleipner CO_2 storage site in the North Sea. The Sleipner CO_2 storage unit is located at approximately 800 m, the minimum required depth for CO_2 injection. Their model can predict CO_2 solubility in brines found in geological conditions as related to CO_2 storage. Portier and Rochelle

(2005) also reported the effect of higher salinity would lower the concentration of dissolved CO_2, and possibly reduce the reaction of CO_2 with the host rock. However, deeper aquifers may have increased temperatures and pressures, which might increase the rate of mineral reactions (Portier and Rochelle, 2005).

All results from these experiments exhibit dissolution of limestone with the injection of CO_2 and saline water. It is probable that limestone dissolution would occur under CO_2 flooding for EOR operations in the saline aquifers of the Williston Basin. The degree to which limestone would dissolve is unknown. The dissolution of limestone results in increased porosity, which in turn can support larger volumes of stored CO_2. However, the integrity of the host rock may be compromised to the point where it becomes unsafe to store CO_2 in the aquifer.

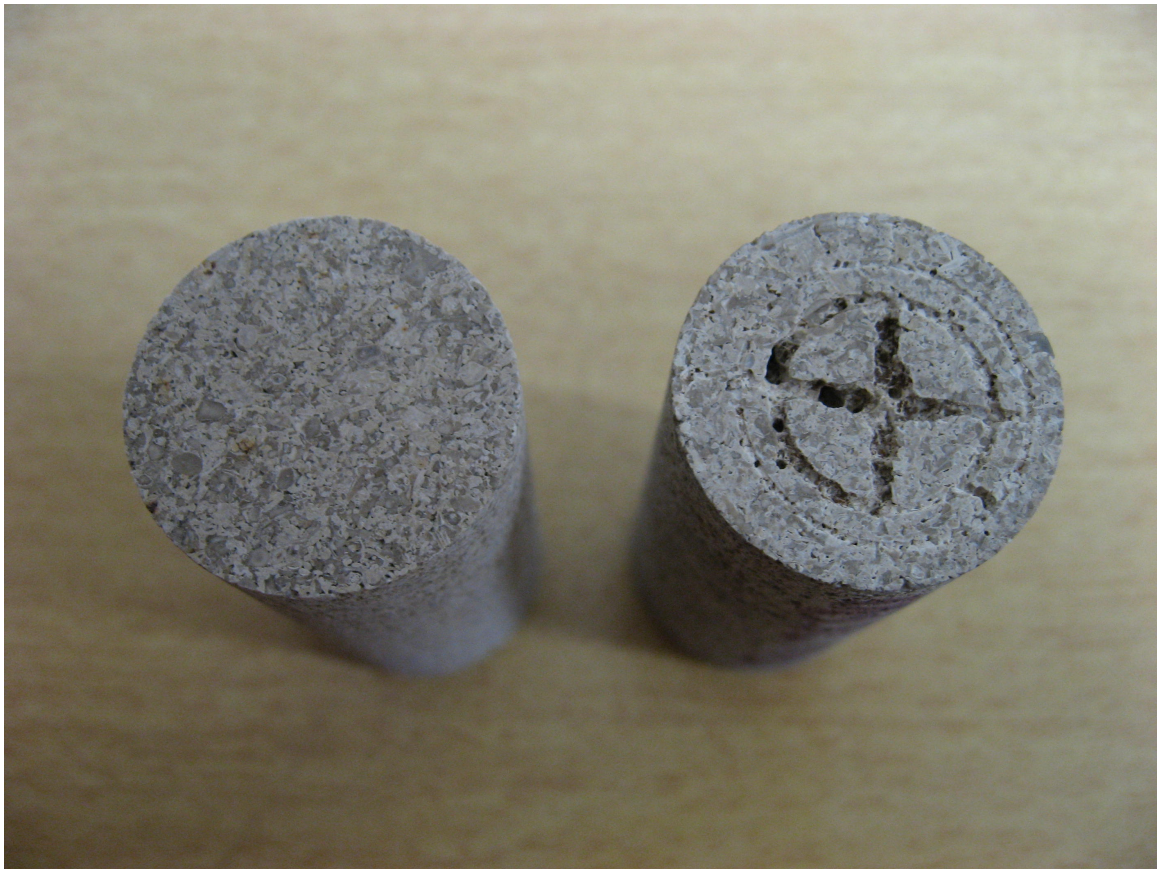

Figure 12. Limestone cores pre- and post-CO_2 flooding. Cores are from the 10,000 ppm experimental run, diameter is 2.54 cm.

CHAPTER VI

CONCLUSIONS

Injection of CO_2 into depleted oil reservoirs of the Williston Basin in North Dakota is being evaluated for the potential to store CO_2 in geologic formations during enhanced oil recovery programs. The extent of how CO_2 reacts with the formation brine and host rock under geologic conditions is unknown. CO_2 reacts with the formation water to form weak carbonic acid. The acidic solution dissolves the carbonate minerals in limestone, releasing calcium and carbonate ions into solution.

Decreased pH and increased conductance measured in the effluent during WAG injections reflect the formation of carbonic acid and subsequent dissolution of carbonate minerals in the limestone. Calcium and bicarbonate ions in solution are an indication of dissolution, as none of the stock solutions initially contained calcium or bicarbonate. The high concentrations of calcium and bicarbonate during the first WAG cycle, followed by decreasing concentrations during later cycles, are an indication that dissolution of carbonate minerals occurs rapidly.

All of the rock cores exhibited decreased density and increased porosity post-WAG flooding, with the exception of the 1,000 ppm saline water flood, in which porosity remained constant. Results from these experiments point to the dissolution of limestone during WAG injections under all concentrations of saline or DI water flood. It is probable that limestone dissolution would occur under CO_2 flooding for EOR operations

in depleted oil reservoirs of the Madison Group in the Williston Basin. The degree to which limestone in the Madison Group would dissolve is unknown. During the first three WAG cycles for all saline and DI water floods, the concentration of calcium in solution was highest for the 100,000 ppm saline solution and decreases with decreasing salinity. Calcium concentration during the first cycle of the 100,000 ppm saline flood was 428 mg/l and the calcium concentration during the first cycle of the DI water flood was 216 mg/l. As the reactions approach equilibrium during the final two cycles, the concentration of calcium decreases for all water floods with a smaller ranger between the highest and lowest concentrations, 127 mg/l for the 10,000 ppm saline flood and 116 mg/l for the DI flood, respectively.

Alkalinity generally follows a similar trend as calcium; the concentration of alkalinity in solution was highest for the 100,000 ppm saline solution and decreases with decreasing salinity over the first three cycles. As CO_2 degassed upon release from the system, alkalinity of the effluent must be considered as estimates. The highest concentration of bicarbonate alkalinity in solution, occurred during the first cycle of the 100,000 ppm saline water flood. As the reactions approach equilibrium during the final cycle, the concentration of alkalinity decreases for all water floods with a smaller range between the highest and lowest concentrations. This trend indicates that CO_2 is more soluble with increasing water salinity, resulting in increased ions in solution. As alkalinity was not present in the stock solutions, the presence of alkalinity in the samples, regardless of concentration, is due to dissolution of calcite minerals in the limestone.

Chemical analyses from all experimental runs show more calcium and bicarbonate ions in solution with increasing salinity of the saline water floods. Increased solubility of CO_2 creates a stronger acid solution, which dissolves more carbonate minerals in the limestone, resulting in increased dissolved ions in solution.

Experimental results obtained in this study indicate that CO_2 is more soluble with increasing salinity. This differs from previous experimental and numerical modeling. Numerous studies have concluded that CO_2 is less soluble with increasing temperatures and increasing salinity. However, CO_2 is also more soluble with increasing pressures. It appears that CO_2 is more soluble in higher salinity waters under higher pressures, such as those found greater than 2200 m below ground. The evidence of increased CO_2 solubility with increased salinity is relevant to pressures and temperatures found in the Madison Group in the Williston Basin.

Based on previous studies, it was predicted that less CO_2 would dissolve with higher salinity water floods. However, based on analytical results during WAG injections of four different saline water concentrations, more CO_2 dissolves in the higher salinity water floods, resulting in increased dissolution of carbonate minerals. Further research is necessary to more accurately predict the behavior of injected CO_2 into the saline aquifers of the Madison Group in the Williston Basin for purposes of CO_2 sequestration or enhanced oil recovery.

APPENDICES

APPENDIX A

Detailed Methodologies

Core Flooding System

Core flooding experiments were conducted in January and February 2009, using a core flooding system and apparatus developed by the Petroleum Engineering Laboratory in the UND Geology and Geological Engineering Department (Figure 3). The core flooding system simulates the carbon dioxide injection process with the capacity to regulate in-situ stress, pressure and temperature exerted on the rock and fluid to simulate subsurface conditions. Pumps alternately or concurrently inject supercritical carbon dioxide and saline water or other fluids. The entire system is controlled and monitored using a computer. The axial and radial stresses, fluid pressure at the inlet and outlet, temperature, flow rate and pump volume are recorded continuously.

A prepared rock core is placed in a rubber core liner extending 12-15 mm beyond the rock core to seal the injected fluid from the confining fluid. The core and liner are placed in the core chamber, which is then sealed. Axial, radial and pore pressures, as well as temperature, can be controlled separately by setting the desired values based on the geological conditions of the formation. Radial in-situ stress can be applied by filling the core chamber assembly with deionized (DI) water at the desired pressure. A piston on the core chamber controls the axial in-situ stress to the sample. The core chamber assembly is enclosed in an oven programmed to maintain a constant temperature.

In these experiments, axial and radial pressures were both set to 4750 psi (32.8 MPa, 323 atm), simulating confining pressure. Pore pressure is held between 2500-2700

psi (17.2 –18.6 MPa, 170-184 atm) using a back-pressure regulator (BPR). The oven temperature was maintained between 135°F and 140°F (57-60°C, 330-333 K). A 40-micron in-line filter was used in place of BPR1 (as shown in Figure 3) to prevent particles in the injection fluids from clogging the pores of the rock. A 40-micron followed by a 2-micron filter were used on the 100,000 ppm flood. The temperature and pressure selected for these experiments are similar to conditions that may be encountered under enhanced oil recovery (EOR) operations in the oil fields of the Madison Group in the North Dakota Williston Basin. The temperature and pressure values were also selected to remain consistent with other research concurrently taking place utilizing this system.

Once the temperature and pressure have stabilized, flooding can begin. ISCO syringe pumps were used to control the pressure and flow rate of fluids through the system. Each pump initially holds approximately 500 ml of fluid or gas. Pump A controls the radial and axial pressures. Pump B controls the injection of carbon dioxide (CO_2) and water (H_2O). Water-alternating-gas (WAG) flooding is conducted at a volumetric rate of 1:2 V_{CO2}: V_{H2O}, with the initial flood of CO_2. One WAG cycle consists of 200 ml of CO_2 and 400 ml of H_2O. Each WAG cycle takes approximately 24 hours to complete. Each experimental run consists of five WAG cycles and takes approximately 5 days to complete. A computer continuously records the date, time, temperature, pressure, pump volume, and flow rate data throughout each experiment, i.e. the data is recorded approximately every six seconds.

Pump B is filled with CO_2 from a compressed gas cylinder and compressed to a volume of 100 milliliters (ml) with a pressure of 2750 psi. CO_2 floods the core at a

constant rate of 0.5 ml/min. This value selected is based on the flow rate a core can withstand without being destroyed as determined by previous experiments using this core flooding system. Due to the physical limitations of the pump, approximately 100 ml of supercritical CO_2 is the maximum volume the pump can hold, resulting in the need to refill the pump with CO_2 to achieve the desired injection volume of 200 ml CO_2 per cycle. The CO_2 effluent is discharged into a plastic container containing 500 ml of DI water, initially. Specific conductance (conductance) and pH are measured approximately every hour of the effluent solution.

Following the CO_2 flood, Pump B is filled with saline water and compressed to a volume of 400 ml. Saline water is injected through the system at a rate of 0.43 ml/min. The effluent of each saline water cycle was collected in a glass jar for laboratory analysis, along with pH and conductivity measurements recorded hourly. The saline effluent was constantly mixed with a magnetic stir bar and stir plate to keep all ions in solution and the sample well mixed for more accurate pH and conductivity readings.

Pump B was rinsed with DI water following saline water flooding. The pump was refilled with DI water and then "scrubbed" by increasing the pressure to 2000 psi and dropping it back to 10 psi, causing the pump to move up and down the cylinder. This is repeated several times until the rinse water came out at an acceptable level for conductivity (Appendix B). The rinse water was collected in 250 ml increments (2 beakers per rinse cycle) and tested with the conductivity meter. A level less than 15 us/cm was considered acceptable for the 1,000 ppm and 10,000 ppm cycles. A level less than 30 uS/cm was considered acceptable after the 100,000 ppm cycles. The pump was thoroughly flushed at the conclusion of the 100,000 ppm test. Due to a delay resulting

from rinsing the pump following the 100,000 ppm flooding cycles, the H_2O flooding rate was increased to between 0.45 and 0.5 ml/min to keep the experiment on schedule.

Rock Core Preparation

Cylindrical rock cores are prepared from a block of quarried Indiana limestone. Each core has a diameter of 2.54 cm, height of 5.08 cm and a mass of approximately 50 g. Each core is given a unique sample number and placed in dry vacuum chamber for one hour to remove all dust particles. While still under a vacuum seal, 800 ml DI water is sucked into the chamber. No longer under a seal, the cores soak in the water for 1 hour. Saturated cores are weighed, dried in an oven, and dry weights are recorded to determine the porosity of the cores. Cores that will be used for saline flooding repeat the vacuum process to soak in saline water prior to flooding experiments. Physical properties of the rock cores are included in Appendix B.

Saline Solution Preparation

Four liters of saline solution were needed for each experimental run. The saline solutions were prepared in the UND Environmental Analytical Research Laboratory (EARL) in Leonard Hall. The saline solutions were prepared using sodium chloride (NaCl) produced by Sigma Chemical Company, Lot 50K0815. The appropriate mass of NaCl was placed in a 2L volumetric flask, filled with DI water and thoroughly mixed. The 2L of solution was placed in a labeled plastic container and a second 2L of solution was prepared for a total of 4L.

Conductance and pH

Conductance and pH were measured in the effluent solution approximately every 60 minutes. A magnetic stir bar and stir plate ensured thorough mixing of the sample. A

Fisher Scientic Accumet Exel, XL meter was programmed to record temperature, pH and conductance at 3600 second intervals. The meter was calibrated according to the manufacturer's specifications.

Laboratory analysis

Effluent samples were collected and preserved following EPA standards. All samples for cations and anions were filtered with a 45-micron glass fiber filter prior to any laboratory testing. All samples were measured within the hold time for each method. Several samples required dilutions in order for the measured concentration to fall within calibration standards. Fresh calibration standards were prepared and analyzed prior to sample analysis for all parameters measured.

Cations

Aqueous samples for laboratory analysis of cations were collected in 100 ml plastic bottles, preserved with 2 ml of nitric acid (HNO_3) to pH<2, and stored in a refrigerator at 4°C. Cations were analyzed by flame atomic absorption (FAA). Fresh calibration standards were prepared and analyzed prior to sample analysis.

Sodium

Sodium samples were predicted to have extremely high concentrations as a result of the NaCl flooding, therefore all sodium samples went through a series of dilutions until the sample was within the calibration range of the FAA. Dilution factors were as high as 20,000, resulting in an increased error.

Calcium

Calcium samples were predicted to have concentrations higher than the calibration range, resulting in dilution of samples. Calcium samples were diluted up to a

dilution factor of 200. After initial analysis of calcium samples, it was determined that the high sodium concentration was causing interference with the calcium analyses. Calcium calibration standards were prepared using a volume of NaCl solution that contained a similar concentration of sodium ions in solution as the samples being analyzed. NaCl was added to the calibration standards for calcium for the 10,000 ppm and 100,000 ppm solutions in order to strengthen the calcium results by having a similar matrix as the standards. Due to differing dilution factors and sodium concentrations in the samples, several sets of calcium standards were prepared.

Iron

Iron analysis was not part of the original analyte list, however, iron appeared during the 100,000 ppm NaCl flood. The iron in solution began precipitating out in the effluent sample jar, suggesting corrosion of the system was taking place. Iron analyses were run on all samples essentially undiluted. Iron was found above method detection limit (MDL) in the samples from the 10,000 ppm and 100,000 ppm flooding tests. While iron concentrations were above the MDL, the concentrations of iron represent less than 0.01% of the total concentration.

Magnesium

Magnesium was not part of the original analyte list and was only tested in three samples to evaluate the need for magnesium analysis. Magnesium standards were prepared using a volume of NaCl solution that contained a similar concentration of sodium ions in solution as the samples being analyzed. Magnesium samples were diluted up to a dilution factor of 2. While magnesium was detected above the MDL in all three of

the samples, the concentrations represent less than 0.02% of the total concentration. Magnesium concentrations improved the ion balance for those three samples.

Anions

Chloride

Chloride was the only anion measured using the ion chromatogram. Samples for anions were collected in 100 ml plastic bottles and stored in a refrigerator at 4°C. Due to the high concentration of chloride resulting from the NaCl flooding, any other anions present in solution would be in trace amounts. Chloride was measured on an ion chromatograph (IC). Fresh calibration standards were prepared and analyzed prior to sample analysis. Chloride samples were diluted up to a dilution factor up to 500.

Chloride results were interpolated from the chromatograph by measuring the area under the peak and correlating that value to the calibration curve. Each sample was measured twice and the average value was used as the concentration for that sample.

Alkalinity

An alkalinity titration was performed on each sample within 24 hours of sample collection. Alkalinity relates to the capacity of water to neutralize acids and is due to the presence of carbonate, bicarbonate and hydroxide ions in the water. Since no carbonates were present in the injection fluid (verified with a titration of the stock solution), the amount of alkalinity in the water is due primarily to the dissolution of the limestone (calcium carbonate) from CO2 and the saline solution. The titrations were performed using a colormetric method with a digital titrator and sulfuric acid. Titration endpoints were verified by testing the pH with a calibrated pH meter.

Carbonates are present at high pH, above 8.3. None of the samples had a pH above 8.3 so the first part of the titration, using Phenolphthalein, was skipped. Since the pH was below 8.3, no hydroxide alkalinity or carbonate alkalinity is present in the sample. All alkalinity is bicarbonate alkalinity (Hach, 2007). Alkalinity was predicted to be about 500 mg/L so a titration endpoint of pH = 4.3 was used per Hach method 8203.

Total Dissolved Solids

Total dissolved solids (TDS) were measured by following the procedure by Hem (1985). Dry beaker tare weights were collected and 100 ml of each sample was placed in a beaker. The beakers were placed in an oven at 103°C overnight and the samples were allowed to completely evaporate. The beakers were placed in a dessicator and allowed to cool to room temperature without re-absorbing water. The beakers were weighed and the TDS was calculated.

APPENDIX B

Detailed Results and Calculations

Table 5: DI rinse of pump B after saline water injection.

Date	Approx. Time	Rinse #	Volume (ml)	Cond (uS/cm)
10,000 ppm NaCl solution				
1/19/09	905	1	0-500	374
		2	0-500	25.08
		3	0-500	8.063
		4	0-500	4.712
		DI water		1.185
1/20/09	952	1	0-200	126
		1	200-400	304.7
		1	400-500	980
		2	0-150	148.5
		2	150-350	78.45
		3	0-200	7.071
		3	200-350	9.118
		3	350-500	8.14
1/21/09	1035	1	0-250	242.3
		1	250-500	342.3
		2	0-250	20.85
		2	250-500	21.90
	1105	3	0-250	7.004
		3	250-500	7.883
1/22/09	1055	1	0-250	344.9
		1	250-500	783.3
		2	0-250	21.88
		2	250-500	24.33
		3	0-250	6.213
		3	250-500	7.779
1/23/09	1105	1	0-250	139.7
		1	250-500	670.4
		2	0-250	30.39
		2	250-500	35.67
		3	0-250	12.10
		3	250-500	9.48
1,000 ppm NaCl solution				
1/26/09	820	1	0-250	56.43
		1	250-500	58.43
		2	0-250	6.128
		2	250-500	5.881
1/27/09	830	1	0-250	42.66
		1	250-500	46.29
		2	0-250	6.813
		2	250-500	7.559
1/28/09	901	1	0-250	52.00
		1	250-500	53.31
		2	0-250	5.172
		2	250-500	5.45
1/29/09	920	1	0-250	48.07

Table 5, continued: DI rinse of pump B after saline water injection.

Date	Approx. Time	Rinse #	Volume (ml)	Cond (uS/cm)
		1	250-500	65.19
		2	0-250	5.195
		2	250-500	8.911
1/30/09	1100	1	0-250	
		1	250-500	
		2	0-250	
		2	250-500	
100,000 ppm NaCl solution				
2/1/09	1010	1	0-250	1553
		1	250-500	3585
		2	0-250	627.7
		2	250-500	1850
		3	0-250	240
		3	250-500	568.9
		4	0-250	95.1
		4	250-500	118
	1110	5	0-250	56.31
		5	250-500	39.11
		6	0-250	21.69
		6	250-500	26.62
2/2/09	920	1	0-250	1332
		1	250-500	3793
		2	0-250	341.2
		2	250-500	1327
		3	0-250	263.4
		3	250-500	772.7
		4	0-250	77.39
		4	250-500	81.3
	1020	5	0-250	19
		5	250-500	19.48
		6	0-250	22.8
		6	250-500	13.77
2/3/09	911	1	0-250	1674
		1	250-500	6028
		2	0-250	751.4
		2	250-500	1189
		3	0-250	129.8
		3	250-500	181.7
		4	0-250	45.5
		4	250-500	60.42
		5	0-250	29.96
	1020	5	250-500	33.12
		6	0-250	22.89
		6	250-500	27.66
2/4/09		1	0-250	600.5

Table 5, continued: DI rinse of pump B after saline water injection.

Date	Approx. Time	Rinse #	Volume (ml)	Cond (uS/cm)
		1	250-500	3264
		2	0-250	520.1
		2	250-500	1704
		3	0-250	290.5
	1015	3	250-500	905.1
		4	0-250	114.5
		4	250-500	221.2
		5	0-250	50.46
		5	250-500	60.88
		6	0-250	22.4
	1110	6	250-500	28.01
2/5/09	1000	1	0-250	1888
		1	250-500	4193
		2	0-250	402.5
		2	250-500	727.1
		3	0-250	235.7
		3	250-500	275.7
		4	0-250	161.1
		4	250-500	174.5
		5	0-250	170.1
		5	250-500	175

Table 6. Properties of rock cores pre- and post-flooding and geomechanical testing.

Pre-Flooding											
No.	Specimen	D	H	V_b	V_p	V_g	W_s	W_d	ρ_g	ρ_d	φ
D	08IL115	2.48	5.04	24.33	3.65	20.68	57.05	53.40	2.58	2.34	0.150
B	08IL116	2.48	5.08	24.53	3.95	20.58	57.70	53.75	2.61	2.35	0.161
A	08IL106	2.48	5.03	24.29	3.80	20.49	57.30	53.50	2.61	2.36	0.156
C	08IL114	2.48	5.02	24.24	3.80	20.44	57.25	53.45	2.62	2.36	0.157
Post-Flooding/Geomechanical Testing											
No.	Specimen	D	H	V_b	V_p	V_g	W_s	W_d	ρ_g	ρ_d	φ
D	08IL115	2.48	5.04	24.33	3.95	20.38	56.15	52.20	2.56	2.15	0.162
B	08IL116	2.48	5.08	24.53	3.95	20.58	56.50	52.55	2.55	2.14	0.161
A	08IL106	2.48	5.03	24.29	3.85	20.44	55.85	52.00	2.54	2.14	0.159
C	08IL114	2.48	5.02	24.24	4.00	20.24	55.70	51.70	2.55	2.13	0.165

D – diameter (cm)
H – height (cm)
V_b – bulk volume (cm^3) = $\pi*(D/2)^2*H$
V_p – pore volume (cm^3) = $W_s - W_d$
V_g – grain volume (cm3) = $V_b - V_p$
W_s – saturated weight (g)
W_d – dry weight (g)
ρ_g – grain density (g/cm^3) = W_d / V_g
ρ_d – bulk (dry) density (g/cm^3)= W_d / V_b
φ - porosity = V_p / V_b

Table 7: Sample IDs and corresponding sample descriptions. Each cycle represents approximately 200 mL of CO_2 injected, followed by 400 mL of saline or deionized water injected.

Sample ID	Sample Description	Total Volume Injected, mL (CO2 + H2O)
A	10,000 ppm stock solution	0
A1	10,000 ppm Cycle 1	600
A2	10,000 ppm Cycle 2	1200
A3	10,000 ppm Cycle 3	1800
A4	10,000 ppm Cycle 4	2400
A5	10,000 ppm Cycle 5	3000
AC	10,000 ppm CO2-DI	3000
B	1,000 ppm stock solution	0
B1	1,000 ppm Cycle 1	600
B2	1,000 ppm Cycle 2	1200
B3	1,000 ppm Cycle 3	1800
B4	1,000 ppm Cycle 4	2400
B5	1,000 ppm Cycle 5	3000
BC	1,000 ppm CO2-DI	3000
C	100,000 ppm stock solution	0
C1	100,000 ppm Cycle 1	600
C2	100,000 ppm Cycle 2	1200
C3	100,000 ppm Cycle 3	1800
C4	100,000 ppm Cycle 4	2400
C5	100,000 ppm Cycle 5	3000
CC	100,000 ppm CO2-DI	3000
D	0 ppm stock solution (DI)	0
D1	0 ppm cycle 1	600
D2	0 ppm cycle 2	1200
D3	0 ppm cycle 3	1800
D4	0 ppm cycle 4	2400
D5	0 ppm cycle 5	3000
DC	0 ppm CO2-DI	3000

Table 8: Dilution factors

Sample ID	Na^+	Ca^{2+}	Fe^{2+}	Cl^-	HCO_3^-	TDS
A	5,000	1	1	50	1	1
A1	5,000	100	1	50	1	1
A2	2,500	100	1	50	1	1
A3	2,500	50	1	50	1	1
A4	2,500	100	1	50	1	1
A5	5,000	10	1	50	1	1
AC	50	1	1	1	1	1
B	250	1	1	5	1	1
B1	250	50	1	5	1	1
B2	250	50	1	5	1	1
B3	250	50	1	5	1	1
B4	250	10	1	5	1	1
B5	250	10	1	5	1	1
BC	25	2	1	1	1	1
C	20,000	1	1	500	1	1
C1	20,000	100	1	500	1	1
C2	20,000	100	1	500	1	1
C3	20,000	100	1	500	1	1
C4	20,000	10	1	500	1	1
C5	20,000	100	1	500	1	1
CC	10,000	1	1	100	1	1
D	1	1	1	1	1	1
D1	1	25	1	1	1	1
D2	1	25	1	1	1	1
D3	1	25	1	1	1	1
D4	1	25	1	1	1	1
D5	1	25	1	1	1	1
DC	1	2	1	1	1	1

Table 9. Quality Control

Sample ID	Ion	Conc SAM	Conc DUP	Conc SPK	% dif	% Rec.
A3D	Ca	2.6334	2.6537		0.38	
C1D	Ca	4.2872	4.41447		1.46	
DCD	Na	1.2116	1.3089		3.86	
A5D	Ca	13.2763	14.2271		3.46	
B3D	Ca	4.446	4.7247		3.04	
C4D	Ca	14.6058	14.6042		0.01	
A5D	Ca	12.7401	13.1813		1.70	
B3D	Ca	4.2322	4.3928		1.86	
C3D	Ca	13.5077	13.5479		0.15	
B3D	Ca	4.2322	3.8238		5.07	
A3D	Na	1.4816	1.3568		4.40	
ACD	Na	0.1295	0.1137		6.50	
C4D	Na	1.9185	1.9509		0.84	
A3D	Fe	0.3442	0.3498		0.81	
B2D	Fe	0.0727	0.0782		3.64	
C2D	Fe	9.8906	9.8573		0.17	
DCD	Fe	0.1342	0.1509		5.86	
D5D	Na	1.042	1.0569		0.71	
C4D	Ca	16.9758	16.5303		1.33	
A3D	Ca	9.7899	10.1731		1.92	
BD	Cl	565.36	549.29		1.44	
C3D	Cl	59456.96	58404.01		0.89	
D2D	Cl	11.42	11.48		0.25	
B3D	Ca	7.9265	8.1842	12.2556	1.60	104.57
D5D	Ca	3.6086	3.7367	9.3383	1.74	103.99
BCS	Na	0.534		0.7334		129.95
AS	Na	0.6931		0.9316		198.25
A4S	Mg	0.9132		0.9426		100.14
BCS	Na	0.5591		1.0285		98.37
A2S	Fe	0.2321		1.4354		76.84
C5S	Fe	1.5056		2.236		73.94
D4S	Fe	0.0626		1.3319		77.41
C1S	Fe	6.6351		6.6254		66.06
D4S	Na	0.634		1.0459		93.49
C3S	Ca	12.4951		16.4613		121.97
ACS	Ca	8.0793		12.9997		114.20
D2S	Cl	11.42		70.87		94.89

Table 10. Values for pH versus pore volume graph.

0 ppm		1,000 ppm		10,000 ppm		100,000 ppm	
Vol	pH	Vol	pH	Vol	pH	Vol	pH
750	6.98	754	6.78	745	6.72	745	6.53
747	6.96	749	6.72	740	6.70	742	6.52
743	7.10	742	6.73	733	6.68	738	6.60
740	6.96	734	6.70	726	6.71	735	6.60
737	6.91	727	6.78	720	6.72	732	6.64
734	6.56	719	6.70	713	6.76	728	6.67
731	6.67	712	6.84	707	6.78	725	6.63
727	6.86	704	6.76	700	6.78	722	6.57
724	7.09	697	6.72	694	6.80	718	6.49
721	7.05	689	6.82	687	6.80	715	6.41
718	6.86	682	6.89	681	6.80	711	6.48
714	6.95	674	6.87	675	6.78	708	6.66
711	6.79	667	6.93	668	6.74	705	6.62
708	7.02	659	6.89	662	6.68	701	6.62
705	6.74	651	5.75	655	6.20	698	6.65
702	7.14	644	4.90	649	4.72	695	6.67
698	6.71	636	5.18	644	4.76	691	6.67
695	6.99	628	5.02	632	4.82	688	6.65
692	6.90	621	5.15	627	4.49	684	6.59
689	7.28	616	5.21	623	4.85	681	6.59
685	7.36	611	5.30	611	4.68	678	6.61
682	7.25	603	5.21	604	5.01	674	6.59
679	7.33	596	5.23	596	6.91	671	6.54
676	6.95	588	6.97	594	6.71	668	6.55
672	7.00	583	6.82	584	6.69	664	6.47
669	7.28	577	6.80	577	6.69	657	5.74
666	6.59	570	6.82	571	6.71	655	4.76
663	6.14	564	6.80	564	6.73	651	4.75
660	4.89	558	6.90	558	6.76	647	4.59
654	5.15	551	6.82	551	6.76	643	4.65
652	4.90	545	6.86	545	6.78	639	4.61
650	5.09	538	6.91	538	6.75	636	4.61
648	4.70	532	6.92	532	6.72	632	4.61
644	5.00	525	6.92	526	6.69	628	4.68
640	5.21	519	6.96	519	6.48	627	4.60
637	4.19	512	6.88	513	5.90	624	4.60
633	4.11	506	6.65	506	5.64	620	4.65
629	4.41	499	4.68	500	4.75	616	4.62
627	5.09	492	4.69	497	4.65	613	4.66
625	5.04	487	5.15	494	4.57	609	4.78
621	4.53	479	4.45	475	4.73	605	6.41
618	4.40	472	4.63	473	4.64	601	6.64
614	5.21	466	4.51	464	4.57	599	7.54
610	4.40	460	5.28	456	4.89	599	7.42
606	6.54	453	4.65	449	6.27	599	7.28
603	6.68	447	7.18	446	6.27	599	6.87

Table 10, continued. Values for pH versus pore volume graph.

0 ppm		1,000 ppm		10,000 ppm		100,000 ppm	
Vol	pH	Vol	pH	Vol	pH	Vol	pH
601	6.87	444	7.26	445	6.26	596	6.82
599	6.79	441	6.93	443	6.15	592	6.85
596	6.57	435	6.88	434	6.17	589	6.85
593	6.56	428	6.92	427	6.17	586	6.86
589	6.86	422	6.87	421	6.21	582	6.86
586	6.50	415	6.89	414	6.25	579	6.86
583	6.64	409	6.89	408	6.23	576	6.84
580	6.92	402	6.98	401	6.25	572	6.82
576	6.91	396	6.97	395	6.27	569	6.82
573	6.63	390	7.00	389	6.27	565	6.82
570	6.91	383	6.89	382	6.30	562	6.83
567	6.89	377	6.89	376	6.29	559	6.79
564	6.66	370	6.86	365	6.32	555	6.79
560	6.99	364	5.64	363	6.71	552	6.83
557	6.83	357	3.71	356	6.11	549	6.83
554	6.77	350	4.95	350	4.74	545	6.86
551	6.81	343	4.49	343	4.60	542	6.85
547	6.85	341	4.19	343	4.39	538	6.83
544	7.04	334	4.98	329	4.73	535	6.82
541	6.77	326	5.02	322	4.72	532	6.79
538	6.70	324	4.95	321	4.47	528	6.82
534	7.08	316	4.47	310	4.73	525	6.75
531	6.83	309	5.04	294	6.33	522	6.80
528	6.65	301	7.08	293	6.30	518	6.76
525	6.73	297	7.35	293	6.18	515	6.45
522	6.96	293	7.03	283	6.19	511	4.58
518	6.81	287	7.02	276	6.21	505	4.76
515	6.57	280	6.96	270	6.23	501	4.73
512	5.81	274	7.01	264	6.23	494	4.63
509	4.86	267	7.01	257	6.27	490	4.62
500	4.63	261	6.99	251	6.26	486	4.63
500	5.03	255	7.02	244	6.27	482	4.61
499	4.31	248	7.03	238	6.28	479	4.61
498	5.12	242	7.04	231	6.33	475	4.64
494	4.67	235	7.06	225	6.35	471	4.58
490	5.24	229	7.07	218	6.38	467	4.61
486	5.25	222	7.03	212	6.46	464	4.62
483	5.05	216	7.01	205	6.81	460	4.59
479	4.80	208	6.92	203	6.51	456	4.62
479	4.47	200	4.50	203	6.08	452	4.86
475	5.02	194	4.50	199	4.39	449	6.64
471	5.08	186	4.57	192	4.51	445	7.47
468	4.96	179	4.98	183	4.36	443	6.82
464	5.20	171	3.87	175	4.52	440	6.83
460	7.07	167	4.83	173	4.24	436	6.83
456	7.05	159	4.22	170	4.44	433	6.83

Table 10, continued. Values for pH versus pore volume graph.

0 ppm		1,000 ppm		10,000 ppm		100,000 ppm	
Vol	pH	Vol	pH	Vol	pH	Vol	pH
453	6.94	152	5.61	158	3.89	430	6.84
451	6.93	144	7.37	151	6.25	426	6.85
448	6.91	142	7.05	149	6.17	423	6.87
445	7.03	136	7.05	148	6.20	420	6.87
442	6.85	130	7.03	148	6.24	416	6.86
439	6.96	123	6.99	142	6.23	413	6.86
435	7.00	117	7.06	136	6.27	409	6.86
432	7.10	110	7.01	129	6.28	406	6.84
429	6.91	104	7.05	123	6.31	403	6.85
426	6.89	97	7.05	116	6.36	399	6.85
423	6.90	91	7.07	110	6.35	396	6.86
419	7.11	84	7.06	104	6.36	393	6.85
416	7.13	78	7.08	97	6.42	389	6.86
413	7.10	71	6.97	91	6.43	386	6.88
410	7.08	65	6.93	84	6.47	382	6.88
406	7.12	59	6.80	78	6.63	379	6.91
403	7.12	53	6.54	71	6.82	376	6.88
400	7.07	47	3.61	65	6.43	372	6.88
397	7.20	44	4.20	61	4.29	369	6.84
394	7.09	41	3.97	48	4.45	366	6.74
390	7.11	34	3.86	40	4.09	362	6.50
387	7.17	28	3.49	33	4.33	359	6.37
384	7.08	20	3.73	25	4.11	355	6.43
381	6.93	13	3.75	21	3.99	352	7.21
377	7.02	5	6.44	16	4.45	349	4.66
374	6.86					345	4.67
371	6.84					344	4.54
368	7.21					342	4.57
365	6.19					339	4.57
361	4.59					335	4.58
353	4.86					331	4.55
351	4.61					329	4.57
348	3.98					328	4.54
344	4.22					327	4.58
340	3.73					324	4.56
336	3.71					320	4.59
333	4.82					316	4.61
329	4.95					312	4.68
328	3.43					309	6.45
324	4.32					305	6.78
320	4.47					302	7.55
317	3.64					299	7.12
313	3.49					297	7.04
309	6.54					289	7.09
305	6.90					282	7.10
302	7.07					274	7.11

Table 10, continued. Values for pH versus pore volume graph.

0 ppm		1,000 ppm		10,000 ppm		100,000 ppm	
Vol	pH	Vol	pH	Vol	pH	Vol	pH
299	6.92					267	7.11
297	7.03					259	7.13
293	6.99					252	7.03
290	6.92					244	7.03
287	7.07					237	7.01
284	7.13					229	6.99
281	7.10					222	6.78
277	6.94					215	5.96
274	6.80					207	5.22
271	7.03					200	4.55
268	7.16					185	4.56
264	7.01					180	4.56
261	6.97					174	4.56
258	7.08					167	4.59
255	7.21					159	4.67
252	7.23					152	7.48
248	7.14					151	7.37
245	7.05					151	7.07
242	7.18					151	7.02
239	7.27					144	7.05
235	7.25					136	7.06
232	7.26					129	7.04
229	7.20					121	7.03
226	6.94					114	6.99
222	7.04					107	6.98
219	7.17					99	6.96
216	6.30					92	6.92
213	4.58					84	6.80
210	4.59					77	6.26
205	3.77					70	4.31
202	5.95					62	4.34
180	3.81					50	4.44
179	3.97					43	4.33
178	3.94					37	5.16
175	3.78					29	4.16
171	3.79					22	4.22
168	4.88					14	4.07
164	3.40						
160	5.11						
156	6.80						
152	7.07						
150	6.92						
147	7.04						
144	6.94						
140	6.96						
137	6.95						

Table 10, continued. Values for pH versus pore volume graph.

0 ppm		1,000 ppm		10,000 ppm		100,000 ppm	
Vol	pH	Vol	pH	Vol	pH	Vol	pH
134	6.96						
131	6.87						
128	7.02						
124	6.97						
121	7.04						
118	6.88						
115	7.03						
111	6.88						
108	6.97						
105	7.02						
102	6.84						
99	6.85						
95	6.95						
92	6.99						
89	6.92						
86	6.92						
82	6.87						
79	6.80						
76	6.85						
73	6.39						
66	7.48						
63	4.37						
60	4.46						
55	4.98						
51	4.92						
47	4.98						
43	4.79						
39	4.59						
36	4.38						
32	3.76						
28	4.82						
27	4.23						
25	4.60						
21	4.06						
18	4.54						
14	4.71						
10	4.69						
6	4.74						
3	5.91						

Table 11. Values for conductance versus pore volume graph. Cond in mS/cm.

0 ppm		1,000 ppm		10,000 ppm		100,000 ppm	
Volume	Cond	Volume	Cond	Volume	Cond	Volume	Cond
750	0.530	749	2.590	745	17.530	745	127.800
747	0.534	742	2.586	740	17.730	742	127.900
743	0.536	734	2.600	733	17.350	738	126.600
740	0.545	727	2.616	726	17.250	735	126.600
737	0.541	719	2.637	720	17.420	732	126.400
734	0.541	712	2.653	713	17.320	728	126.900
731	0.560	704	2.674	707	17.250	725	126.900
727	0.575	697	2.665	700	16.710	722	126.900
724	0.582	689	2.344	694	16.660	718	126.900
721	0.592	682	2.405	687	14.800	715	126.900
718	0.600	674	2.461	681	14.800	711	126.600
714	0.610	667	2.519	675	14.360	708	126.400
711	0.621	659	1.478	668	8.027	705	125.000
708	0.632	644	0.344	662	3.547	701	121.300
705	0.625	636	0.343	649	0.668	698	120.100
702	0.633	628	0.336	644	0.720	695	107.200
698	0.576	621	0.326	632	0.667	691	107.200
695	0.593	616	0.324	627	0.612	688	107.200
692	0.620	611	0.321	623	0.600	684	106.500
689	0.648	603	0.319	611	0.591	681	104.400
685	0.676	596	0.313	596	17.980	678	89.630
682	0.711	588	2.814	594	17.860	674	68.980
679	0.756	583	2.807	584	17.870	671	45.410
676	0.715	577	2.819	577	17.770	668	8.048
672	0.481	570	2.840	571	17.800	661	0.001
669	0.332	564	2.869	564	17.920	655	6.550
660	0.210	558	2.892	558	17.840	651	6.500
654	0.220	551	2.921	551	17.120	647	6.491
652	0.220	545	2.847	545	16.960	643	6.480
650	0.220	538	2.862	538	15.030	639	6.478
648	0.219	532	2.585	532	15.040	636	6.467
644	0.219	525	2.651	526	14.720	632	6.409
640	0.217	519	2.511	519	7.647	628	6.346
637	0.220	512	1.677	513	0.018	627	6.325
633	0.212	506	0.253	506	0.001	624	6.350
629	0.212	492	0.295	500	0.546	620	6.315
627	0.212	487	0.296	497	0.546	616	6.296
625	0.212	479	0.292	494	0.558	613	6.319
621	0.210	472	0.289	475	0.501	609	6.316
618	0.210	466	0.295	473	0.501	605	130.000
614	0.210	460	0.290	464	0.478	601	129.600
610	0.209	453	0.283	456	0.467	599	129.300
606	0.724	441	3.016	449	18.220	599	129.200
603	0.726	441	3.014	446	18.370	599	128.100
601	0.727	441	3.035	445	18.190	599	126.300
599	0.723	435	3.043	443	17.840	596	130.300

Table 11, continued. Values for conductance versus pore volume injected graph. Cond in mS/cm.

0 ppm		1,000 ppm		10,000 ppm		100,000 ppm	
Volume	Cond	Volume	Cond	Volume	Cond	Volume	Cond
596	0.727	428	3.072	434	17.880	592	130.300
593	0.732	422	3.080	427	17.650	589	130.300
589	0.743	415	3.099	421	17.750	586	130.300
586	0.755	409	3.120	414	17.660	582	130.300
583	0.762	402	3.009	408	17.730	579	130.300
580	0.770	396	2.680	401	17.680	576	130.000
576	0.776	390	2.718	395	16.890	572	130.000
573	0.793	383	2.755	389	14.830	569	129.900
570	0.805	377	2.151	382	15.070	565	129.900
567	0.816	370	0.777	376	14.830	562	129.900
564	0.828	364	0.006	365	9.877	559	129.300
560	0.843	343	0.228	363	0.004	555	128.100
557	0.853	341	0.227	356	0.006	552	122.500
554	0.844	334	0.226	350	0.519	549	108.500
551	0.855	326	0.225	343	0.420	545	108.100
547	0.868	324	0.224	343	0.416	542	108.300
544	0.803	316	0.221	329	0.416	538	108.300
541	0.824	309	0.218	322	0.423	535	107.800
538	0.858	301	3.242	310	0.406	532	107.300
534	0.901	297	3.222	294	17.910	528	105.300
531	0.952	293	3.197	293	17.860	525	88.700
528	0.999	287	3.218	293	17.440	522	62.910
525	0.925	280	3.252	283	17.540	518	27.560
522	0.696	274	3.284	276	17.680	515	0.312
518	0.536	267	3.323	270	17.600	511	0.022
515	0.437	261	3.377	264	17.690	505	6.005
509	0.207	255	3.391	257	17.670	501	6.006
500	0.193	248	3.323	251	17.620	494	6.060
500	0.192	242	3.362	244	17.450	490	6.029
499	0.194	235	3.067	238	15.070	486	6.045
498	0.192	229	3.175	231	15.040	482	5.690
494	0.191	222	2.550	225	14.970	479	5.661
490	0.192	216	1.317	218	13.830	475	5.652
486	0.188	200	0.182	212	7.091	471	5.628
483	0.184	194	0.200	199	0.003	467	5.644
479	0.175	186	0.202	192	0.356	464	5.655
479	0.175	179	0.177	183	0.348	460	5.624
475	0.174	171	0.065	175	0.267	456	5.619
471	0.173	167	0.174	173	0.260	452	5.467
468	0.171	159	0.175	170	0.235	449	127.300
464	0.170	152	0.162	158	0.211	445	126.900
456	0.997	144	3.180	151	0.161	443	128.400
453	1.004	142	3.139	149	17.870	440	128.500
451	1.060	136	3.158	148	17.510	436	128.700
448	1.072	130	3.189	148	17.840	433	128.700

Table 11, continued. Values for conductance versus pore volume injected graph. Cond in mS/cm.

0 ppm		1,000 ppm		10,000 ppm		100,000 ppm	
Volume	Cond	Volume	Cond	Volume	Cond	Volume	Cond
445	1.079	123	3.229	142	18.040	430	128.500
442	1.091	117	3.268	136	18.180	426	128.500
439	1.114	110	3.324	129	18.120	423	128.500
435	1.131	104	3.378	123	18.110	420	128.300
432	1.151	97	3.431	116	18.120	416	128.300
429	1.158	91	3.400	110	17.940	413	128.300
426	1.183	84	3.169	104	17.740	409	128.200
423	1.211	78	3.282	97	17.000	406	128.100
419	1.232	71	3.318	91	15.180	403	127.700
416	1.253	65	2.402	84	14.780	399	126.400
413	1.280	59	1.388	78	13.750	396	122.100
410	1.293	47	0.120	71	8.593	393	121.200
406	1.277	49	0.118	65	0.122	389	108.100
403	1.300	41	0.118	48	0.148	386	108.100
400	1.300	34	0.110	40	0.139	382	107.600
397	1.230	28	0.109	33	0.125	379	106.600
394	1.266	20	0.108	25	0.108	376	101.700
390	1.324	13	0.105	21	0.104	372	80.570
387	1.382	5	0.086	16	0.094	369	59.270
384	1.439			9	0.048	366	35.150
381	1.413					362	1.691
377	1.123					355	0.010
374	0.905					349	5.407
371	0.670					345	5.410
368	0.257					344	5.359
361	0.179					342	5.382
353	0.162					339	5.369
351	0.160					335	5.345
348	0.162					331	5.357
344	0.161					329	5.329
340	0.161					328	5.329
336	0.159					327	5.326
333	0.139					324	5.293
329	0.139					320	5.285
328	0.139					316	5.253
324	0.139					312	5.234
320	0.139					309	130.400
317	0.137					305	130.200
313	0.137					302	130.000
309	0.129					299	127.800
305	1.061					297	127.700
302	1.069					289	127.500
299	1.074					282	127.500
297	1.146					274	127.500
293	1.165					267	126.900

Table 11, continued. Values for conductance versus pore volume injected graph. Cond in mS/cm.

0 ppm		1,000 ppm		10,000 ppm		100,000 ppm	
Volume	Cond	Volume	Cond	Volume	Cond	Volume	Cond
290	1.174					259	121.600
287	1.192					252	120.700
284	1.209					244	106.300
281	1.228					237	105.200
277	1.250					229	67.060
274	1.269					222	0.339
271	1.289					200	4.854
268	1.312					185	4.861
264	1.339					180	4.861
261	1.346					174	4.879
258	1.347					167	4.812
255	1.374					159	4.506
252	1.412					152	127.100
248	1.448					151	127.600
245	1.345					151	126.300
242	1.409					151	127.100
239	1.449					144	126.700
235	1.453					136	126.600
232	1.219					129	126.100
229	1.046					121	120.300
226	0.884					114	119.200
222	0.665					107	103.700
219	0.128					99	103.400
213	0.130					92	81.010
210	0.128					84	30.660
205	0.121					77	26.120
202	0.121					70	0.002
198	0.146					62	1.521
195	0.146					50	1.470
191	0.146					43	1.401
187	0.146					37	1.205
183	0.146					29	1.170
180	0.150					22	1.051
179	0.104					14	0.882
178	0.103					6	0.258
175	0.102						
171	0.098						
168	0.094						
164	0.092						
160	0.089						
156	1.236						
152	1.244						
150	1.276						
147	1.288						
144	1.314						

Table 11, continued. Values for conductance versus pore volume injected graph. Cond in mS/cm.

0 ppm		1,000 ppm		10,000 ppm		100,000 ppm	
Volume	Cond	Volume	Cond	Volume	Cond	Volume	Cond
140	1.337						
137	1.354						
134	1.377						
131	1.398						
128	1.426						
124	1.448						
121	1.481						
118	1.509						
115	1.546						
111	1.570						
108	1.531						
105	1.414						
102	1.453						
99	1.495						
95	1.542						
92	1.619						
89	1.691						
86	1.786						
82	1.873						
79	1.850						
76	1.225						
73	0.164						
63	0.085						
60	0.085						
55	0.084						
51	0.085						
47	0.082						
43	0.078						
39	0.073						
36	0.075						
32	0.067						
28	0.065						
27	0.064						
25	0.065						
21	0.063						
18	0.062						
14	0.061						
10	0.054						
3	0.012						

Table 12. Water density calculations. Weight in g.

Soln.	Wt. 1 mL	Soln.	Wt. 1 mL
0	0.9948	1000	0.9973
ppm	0.9928	ppm	0.9800
	0.9861		0.9869
	1.0114		0.9851
	0.9865		0.9928
Average	0.9943	Average	0.9884
Soln.	wt 1 mL	Soln.	wt 1 mL
10000	1.0034	100000	1.0619
ppm	1.0025	ppm	1.0557
	0.9962		1.0533
	1.0036		1.0547
	1.0000		1.0542
Average	1.0011	Average	1.0560

APPENDIX C

Oil Fields in the Madison Group

ALEXANDER
ANTELOPE
ANTELOPE CREEK
ANTLER
ARNEGARD
ASSINIBOINE
AURELIA
AVOCA
BADEN
BAKER
BANKS
BANNER
BAR BUTTE
BARTA
BATTLEVIEW
BAUKOL NOONAN
BAUMANN DRAIN
BEAR CREEK
BEAR DEN
BEARS TAIL
BEAVER CREEK
BEAVER LODGE
BEICEGEL CREEK
BENNETT CREEK
BERG
BERTHOLD
BICENTENNIAL
BIG DIPPER
BIG STICK
BLACK SLOUGH
BLACKTAIL
BLAINE
BLUE BUTTES
BLUELL
BOUNDARY CREEK
BOWBELLS
BOWLINE
BOXCAR BUTTE
BRIAR CREEK
BROOKLYN
BUCKHORN
BUFFALO WALLOW
BUFORD
BULL BUTTE
BULL CREEK
BULL MOOSE
BULL RUN
BULLSNAKE
BUTTE
CABERNET
CAMEL BUTTE
CAMP
CAPA
CARTER
CARTWRIGHT
CATWALK
CEDAR CREEK
CENTENNIAL
CHARLSON
CHATEAU
CHOLA
CHURCH
CIMBEL
CLAY
CLAYTON
CLEAR CREEK
CLEAR WATER
COLQUHOUN
COLUMBUS
CORINTH
COTEAU
COULEE
COW CREEK
CRAZY MAN CREEK
CROFF
CROOKED CREEK
CROSBY
CULVER
CUSTOMS
CUTBANK CREEK
DALE
DANCE CREEK
DANEVILLE
DAVIS CREEK
DELTA
DES LACS
DEVILS PASS
DICKINSON
DIMMICK LAKE
DIMOND
DOLPHIN
DONNYBROOK
DORE
DRY CREEK
DUBLIN
DUCK CREEK
EAST FORK
EAST GOOSE LAKE
EAST TIOGA
EDEN VALLEY
EDGE
EIDSVOLD
EIGHTMILE
ELAND
ELK
ELKHORN RANCH
ELMORE
ELMS
ENTRY
EPPING
ESTES
FANCY BUTTES
FLAT LAKE EAST
FLAT TOP BUTTE
FLAXTON
FOOTHILLS
FOREMAN BUTTE
FOUR EYES
FRYBURG
FT. BUFORD
GARDEN
GAYLORD
GLASS BLUFF
GLENBURN
GOOD LUCK
GRASSLAND
GRASSY BUTTE
GREAT NORTHERN
GREEN LAKE
GREENBUSH
GREENE
GRENORA
GRINNELL
GROS VENTRE
GROVER

HAAS
HAMLET
HANKS
HARAM
HARDING
HARDSCRABBLE
HARTLAND
HAWKEYE
HAY CREEK
HAY DRAW
HAYLAND
HEART BUTTE
HEBRON
HEDBERG
HILINE
HOFFLUND
HULSE COULEE
HUNGRY MAN BUTTE
HURLEY
INDIAN HILL
IVANHOE
JOHNSON CORNER
KANE
KANU
KEENE
KILLDEER
KIMBERLY
KNUTSON
KUROKI
LAKE DARLING
LAKE ILO
LAKE TRENTON
LAKE VIEW
LAKESIDE
LANDA
LANSFORD
LARSON
LAST CHANCE
LEONARD
LESJE
LIGNITE
LINDAHL
LITTLE BUTTE
LITTLE DEEP CREEK
LITTLE KNIFE
LIVESTOCK
LOCKWOOD
LONE BUTTE
LONE TREE
LONESOME
LONG CREEK
LORAINE
LOST BRIDGE
LOSTWOOD
LUCKY MOUND
LUCY
MACKOBEE COULEE
MAD MAX
MANDAN
MANDAREE
MANNING
MARMON
MARQUIS
MARY
MCGREGOR
MCKINNEY
MEDORA
MIDDLE CREEK
MIDWAY
MINNESOTA
MISSOURI RIDGE
MOHALL
MONDAK
MORAINE
MORGAN DRAW
MOUNTROSE
MOUSE RIVER PARK
NAMELESS
NEW HOME
NIOBE
NOHLY LAKE
NOONAN
NORMA
NORTH BRANCH
NORTH ELKHORN
RANCH
NORTH GRANO
NORTH HAAS
NORTH MAXBASS
NORTH MOUSE RIVER
PARK
NORTH SERGIS
NORTH SOURIS
NORTH STAR
NORTH TIOGA
NORTH WESTHOPE
NORTHEAST FOOTHILLS
NORTHEAST LANDA
NORTHWEST MCGREGOR
NORWEGIAN CREEK
OAKDALE
OSLOE
PAINTED WOODS
PARK
PASSPORT
PATENT GATE
PAULSON
PERELLA
PERSHING
PICKETT
PIERRE CREEK
PLAZA
PLEASANT
PLEASANT VALLEY
POE
POKER JIM
PORTAL
POWERS LAKE
PRAIRIE JUNCTION
PRATT
PRESCOTT
PRONGHORN
RAGGED BUTTE
RANDOLPH
RAUB
RAWSON
RED WING CREEK
REFUGE
RENNIE LAKE
RENVILLE
RICHBURG
RIDER
RIVAL
ROCKY HILL
ROCKY RIDGE

ROOSEVELT
ROSEBUD
ROTH
ROUGH RIDER
ROUND TOP BUTTE
RUSSELL
RUSSIAN CREEK
SADDLE BUTTE
SADLER
SAKAKAWEA
SATHER LAKE
SCAIRT WOMAN
SCANDIA
SCOTIA
SERGIS
SEVENMILE COULEE
SHEALEY
SHERMAN
SHERWOOD
SHOCKLEY
SHORT CREEK
SIMON BUTTE
SIOUX
SIXMILE
SKABO
SMITH
SNOW
SNOWCOVER
SOURIS
SOUTH ANTLER CREEK
SOUTH BOXCAR
SOUTH BULL MOOSE
SOUTH COTEAU
SOUTH HAAS
SOUTH LANDA
SOUTH LONE TREE
SOUTH PLEASANT
SOUTH STARBUCK
SOUTH WESTHOPE
SOUTHWEST AURELIA
SOUTHWEST HAAS
SOUTHWEST LANDA
SOUTHWEST STARBUCK
SPIRAL
SPOTTED HORN
SPRING COULEE
SPRING VALLEY
SPRINGBROOK
SQUARE BUTTE
SQUAW CREEK
SQUAW GAP
ST. JACOBS
STADIUM
STAFFORD
STAMPEDE
STANLEY
STARBUCK
STINSON
STOCKYARD CREEK
STONEVIEW
STONY CREEK
STONY RUN
SUBDIVISION
SUGAR BEET
T. R.
TEMPLE
THOMPSON LAKE
TIMBER CREEK
TIOGA
TOBACCO GARDEN
TODD
TOLLEY
TORNING
TRAILSIDE
TREE TOP
TRURO
UKRAINA
UNION CENTER
UPPER DES LACS
VALLEY ROAD
VANVILLE
VERSIPPI
VIKING
WABEK
WAKE
WARD
WAYNE
WERNER
WEST BANK
WEST BUTTE
WEST CAPA
WEST DICKINSON
WEST GREENE
WEST ROTH
WEST SHERWOOD
WEST TIOGA
WESTHOPE
WHEATON
WHISKEY JOE
WHITE ASH
WHITE EARTH
WHITE LAKE
WILDROSE
WILEY
WILLIAMS CREEK
WILLISTON
WILLMEN
WILLOW CREEK
WINDMILL
WINTER BUTTE
WOBURN
ZION

REFERENCES

Allen, D., Strazisar, B., Soong, Y., Hedges, S. 2005. Modeling carbon dioxide sequestration in saline aquifers: Significance of elevated pressures and salinities. Fuel Processing Technology, 86 (14-15), 1569-1580.

Andre, L, Audigane, P, Azaroual, M., Menjoz, A. 2007. Numerical modeling of fluid-rock chemical interactions at the supercritical CO_2 liquid interface during CO_2 injection into a carbonate reservoir, the Dogger aquifer (Paris Basin, France). Energy Conversion Management, 48 (6), 1782-1797.

Bachu, S. 2000. Sequestration of CO_2 in geological media: criteria and approach for site selection in response to climate change. Energy Conversion Management, 41 (9), 953– 970.

Bachu, S. 2003. Screening and ranking of sedimentary basins for sequestration of CO_2 in geological media in response to climate change. Environmental Geology, 44 (3), 277– 289.

Bachu, S., Adams, J. 2003. Sequestration of CO_2 in geological media in response to climate change: capacity of deep saline aquifers to sequester CO_2 in solution. Energy Conversion Management, 44 (20), 3151–3175.

Bachu, S., Bonijoly, D., Bradshaw, J., Burruss, R., Holloway, S., Christensen, N., Mathiassen, O. 2007. CO_2 storage capacity estimation: methodology and gaps. International Journal of Greenhouse Gas Control, 1 (4), 430-443.

Bachu, S., Gunter, W., and Perkins, E. 1994. Aquifer disposal of CO_2: Hydrodynamic and mineral trapping. Energy Conversion Management, 35 (4), 269-279.

Bachu, S., Hitchon, B. 1996. Regional-scale flow of formation waters in the Williston Basin. AAPG Bulletin, 80, 248–264.

Bateman, K., Turner, G., Pearce, J., Noy, D., Birchall, D., Rochelle, C. 2005 Large-Scale Column Experiment: Study of CO_2, Porewater, Rock Reactions and Model Test Case. Oil & Gas Science and Technology – Rev. IFP, 60 (1), 161-175.

Bergman, P., Winter, E. 1995. Disposal of carbon dioxide in aquifers in the U.S. Energy Conversion Management, 36 (6-9), 523-526.

Birkholzer, J., Zhou, Q., Tsang, C. 2009. Large-scale impact of CO_2 storage in deep saline aquifers: A sensitivity study on pressure response in stratified systems. International Journal of Greenhouse Gas Control, 3 (2), 181-194.

Bluemle, J., Anderson, S., Andrew, J., Fischer D., LeFever, J., 1986. North Dakota Stratigraphic Column, North Dakota Geological Survey. Miscellaneous Series #66. Blunt, M., Fayers, F., Orr, Jr, F. 1993. Carbon dioxide in enhanced oil recovery. Energy Conversion Management, 34 (9-11), 1197-1204.

Busby, J., Kimball, B., Downey, J., Peter, K. 1995. Geochemistry of water in aquifers and confining units of the Northern Great Plains in parts of Montana, North Dakota, South Dakota, and Wyoming. U.S. Geological Survey Professional Paper 1402-F, p. F1-F146.

Carr, T., Wickstron, L., Korose, C., Fisher, R., Solano-Acosta, W., Eaton, N. 2003. Online tools to evaluate saline aquifers for CO_2 sequestration. Kansas Geological Survey Open-File Report 2003-33.

Downey, J. 1984. Geohydrology of the Madison and associated aquifers in parts of Montana, North Dakota, South Dakota, and Wyoming, U.S. Geological Survey Professional Paper 1273-G, p. G1–G47.

Downey, J. 1986. Geohydrology of bedrock aquifers in the Northern Great Plains in parts of Montana, North Dakota, South Dakota, and Wyoming, U.S. Geological Survey Professional Paper 1402-E, p. E1–E87.

Downey, J. Dinwiddie, G. 1988. The Regional aquifer system underlying the Northern Great Plains in parts of Montana, North Dakota, South Dakota, and Wyoming – summary. U.S. Geological Survey Professional Paper 1402-A, p. A1-A64.

Duan, Z., Sun, R. 2003. An improved model calculating CO_2 solubility in pure water and aqueous NaCl solutions form 273 to 533 K and from 0 to 2000 bar. Chemical Geology, 193 (3-4), 257-271.

Emberley, S., Hutcheon, I., Shevalier, M., Durocher, K., Mayer, B., Gunter, W., Perkins, E. 2005. Monitoring of fluid-rock interaction and CO_2 storage through produced fluid sampling at the Weyburn CO_2-injection enhanced oil recovery site, Saskatchewan, Canada. Applied Geochemistry, 20 (6), 1131-1157.

Enting, I., Etheridge, D., Fielding, M. 2008. A perturbation analysis of the climate benefit from geosequestration of carbon dioxide. International Journal of Greenhouse Gas Control, 2 (3), 289-296.

Finneran, D., Morse, J. 2009 Calcite dissolution kinetics in saline waters. Chemical Geology, 268 (1-2), 137-146.

Fischer, D., LeFever, J., LeFever, R., Anderson, S., Helms, L., Whittaker, S., Sorensen, J., Smith, S., Peck, W., Steadman, E., Harju, J. 2005a. Overview of Williston Basin Geology as it relates to CO_2 sequestration. Plains CO_2 Reduction Partnership Report, University of North Dakota Energy and Environmental Research Center, Grand Forks, North Dakota, USA.

Fischer, D., LeFever, J., LeFever, R., Helms, L., Sorensen, J., Smith, S., Steadman, E., Harju, J. 2005b. Mission Canyon Formation Outline. Plains CO_2 Reduction Partnership Report, University of North Dakota Energy and Environmental Research Center, Grand Forks, North Dakota, USA.

Fischer, D., Smith, S., Peck, W., LeFever, J., LeFever, R., Helms, L., Sorensen, J., Steadman, E., Harju, J. 2005c. Sequestration potential of the Madison of the Northern Great Plains aquifer system (Madison Geological Sequestration Unit). Plains CO_2 Reduction Partnership Report, University of North Dakota Energy and Environmental Research Center, Grand Forks, North Dakota, USA.

Gaus, I., Audigane, P., Andre, L., Lions, J., Jacquemet, N., Durst, P., Czernichowski-Lauriol, I., Azaroual, M. 2008. Geochemical and solute transport modeling for CO_2 storage, what to expect from it? International Journal of Greenhouse Gas Control, 2 (4), 605-625.

Gerhard, L., Anderson, S., LeFever, J., Carlson, C. 1982. Geological development, origin, and energy mineral resources of the Williston Basin, North Dakota. North Dakota Geological Survey Miscellaneous Series 63. Bismarck, ND, USA.

Giammar, D., Bruant Jr., R., Peters, C. 2005. Forsterite dissolution and magnesite precipitation at conditions relevant for deep saline aquifer storage and sequestration of carbon dioxide. Chemical Geology, 217 (3-4), 257-276.

Gledhill, D., Morse, J. 2006. Calcite solubility in Na-Ca-Mg-Cl brines. Chemical Geology, 233 (3-4), 249-256.

Grigg, R., Svec, R., Zeng, Z., Bai, B., Liu, Y. 2005. Improving CO_2 efficiency for recovering oil in heterogeneous reservoirs. Final report for DOE Contract No. DE-FG26-01BC15364, New Mexico Petroleum Recovery Research Center, Socorro, NM.

Gunter, W., Perkins, E., Hutcheon, I. 2000. Aquifer disposal of acid gases: modelling of water–rock reactions for trapping of acid wastes. Applied Geochemistry, 15 (8), 1085– 1095.

Gunter,W., Wiwchar, B., Perkins, E. 1997. Aquifer disposal of CO_2-rich greenhouse gases: extension of the time scale of experiment for CO_2-sequestering reactions by geochemical modelling. Mineralogy and Petrology, 59 (1–2), 121– 140.

Hach Company. 2007. Alkalinity method 8203 by digital titrator, DOC316.53.01155, Instrument Manual.

Heck, T. 1979. Depositional environments and diagenesis of the Mississippian Bottineau Interval (Lodgepole) in North Dakota: University of North Dakota Unpublished Master's Thesis, p. 227.

Hem, J. 1985. Study and interpretation of the chemical characteristics of natural water. USGS Water-Supply Paper 2254, p. 263.

Hitchon, B. 2000. 'Rust' contamination of formation waters from producing wells. Applied Geochemistry, 15 (10), 1527-1533.

Hitchon, B., Gunter, W., Gentzis, T., Bailey, R. 1999. Sedimentary basins and greenhouse gases: a serendipitous association. Energy Conversion Management, 40 (8), 825–843.

Holloway, S. 1997. An overview of the underground disposal of carbon dioxide. Energy Conversion Management, 38 (SS), S193–S198.

Holloway, S., Savage, D. 1993. The potential for aquifer disposal of carbon dioxide in the UK. Energy Conversion Management, 34 (9-11), 925-32.

Holtz, M., Nance, P., Finley, R. 2001. Reduction of greenhouse gas emissions through CO_2 EOR in Texas. Environmental Geosciences, 8 (3), 187-199.

Izgec, O., Demiral, B., Bertin, H., Akin, S. 2008. CO_2 injection into saline carbonate aquifer formations I: laboratory investigation. Transport in Porous Media, 72 (1), 1-24.

Jiang, C., Li, M., Osadetz, K., Snowdon, L., Obermajer, M., Fowler, M. 2001. Bakken/Madison petroleum systems in the Canadian Williston Basin. Part 2: molecular markers diagnostic of Bakken and Lodgepole source rocks. Organic Geochemistry, 32, 1037-1054.

Kaszuba, J., Janecky, D., Snow, M. 2003. Carbon dioxide reaction processes in a model brine aquifer at 200 °C and 200 bars: implications for geologic sequestration of carbon. Applied Geochemistry, 18 (7), 1065-1080.

Kaszuba, J., Janecky, D., Snow, M. 2005. Experimental evaluation of mixed fluid reactions between supercritical carbon dioxide and NaCl brine: Relevance to the integrity of a geologic carbon repository. Chemical Geology, 217 (3-4), 277-293.

Ketzer, R., Iglesias, R., Einloft, S., Dullius, J., Ligabue, R., de Lima, V. 2009. Water-rock-CO_2 interactions in saline aquifers aimed for carbon dioxide storage: Experimental and numerical modeling studies of the Rio Bonito Formation (Permian), southern Brazil. Applied Geochemistry, 24 (5), 760-767.

Kharaka, Y., Thordsen, J., Hovorka, S., Nance, H., Cole, D., Phelps, T., Knauss, K. 2009. Potential environmental issues of CO_2 storage in deep saline aquifers: Geochemical results from the Frio-I Brine Pilot test, Texas, USA. Applied Geochemistry, 24 (6), 1106-1112.

Lagneau, V., Pipart, A., Catalette, H. 2005. Reactive transport modelling of CO_2 sequestration in deep saline aquifers. Oil Gas Science and Technology, 60 (2), 231–247.

Law, D., Bachu, S. 1996. Hydrogeological and numerical analysis of CO_2 disposal in deep aquifers in the Alberta Sedimentary Basin. Energy Conversion Management, 37 (6-8), 1167-1174.

LeFever, J., LeFever R. 2005. Salts in the Williston Basin, North Dakota. NDGS Report of Investigations No. 103.

LeFever, R. 1998. Hydrodynamics of Formation Waters in the North Dakota Williston Basin. Eighth International Williston Basin Symposium, Saskatchewan Geological Society Special Publication No. 13, p. 229-237.

LeFever, R. 2009. Personal Correspondence.

McGee, E. 1989. Mineralogical Characterization of the Shelburne Marble and the Salem Limestone – Test Stones Used to Study the Effects of Acid Rain. U. S. Geological Survey Bulletin, Report: B 1889, p. 25.

Nelms, R., Burke, R. 2004. Evaluation of oil reservoir characteristics to assess North Dakota carbon dioxide miscible flooding potential. 12th Williston Basin Horizontal Well and Petroleum Conference May 2-4, Minot, ND, USA.

Oruganti, Y., Bryant, S. 2009. Pressure build-up during CO2 storage in partially confined aquifers. Energy Procedia, 1 (1), 3315-3322.

Pawar, R., Zhang, D., Westrich, J., Grigg, R., and Stubbs, B. 2002. Geological Sequestration of Carbon Dioxide in a Depleted Oil Reservoir. Paper 75256 presented at the SPE/DOE Thirteenth Symposium on Improved Oil Recovery, Tulsa, April 13-17, 2002.

Portier, S., Rochelle, C. 2005. Modelling CO_2 solubility in pure water and NaCl-type waters from 0 to 300 °C and from 1 to 300 bar Application to the Utsira Formation at Sleipner. Chemical Geology, 217 (3-4), 187-199.

Preston, C., Monea, M., Jazrawi, W., Brown, K., Whittaker, S., White, D., Law, D., Chalaturnyk, R., Rostron, B. 2005. IEA GHG Weyburn $CO2_2$ monitoring and storage project. Fuel Processing Technology, 86 (14-15), 1547-1568.

Qi, R., LaForce, T., Blunt, M. 2009. Design of carbon dioxide storage in aquifers. International Journal of Greenhouse Gas Control, 3 (2), 195-205.

Rosenbauer, R., Koksalan, T., Palandri, J. 2005. Experimental investigation of CO_2–brine–rock interactions at elevated temperature and pressure: Implications for CO_2 sequestration in deep-saline aquifers. Fuel Processing Technology, 86, 1581–1597.

Shiraki, R., Dunn, T. 2000. Experimental study on water–rock interactions during CO_2 flooding in the Tensleep Formation, Wyoming, USA. Applied Geochemistry, 15 (3), 265–279.

Smith, N. 1966. Sedimentology of the Salem Limestone in Indiana. The Ohio Journal of Science, 66 (2) 168-179.

Solomon, S., Carpenter, M., Flach, T. 2008. Intermediate storage of carbon dioxide in geological formations: A technical perspective. International Journal of Greenhouse Gas Control, 2 (4), 502-510.

Soong, Y., Goodman, A., McCarthy-Jones, J., Baltrus, J. 2004. Experimental and simulation studies on mineral trapping of CO_2 with brine. Energy Conversion Management, 45 (11-12), 1845–1859.

Spycher, N., Pruess, K. 2005. CO_2-H_2O mixtures in the geological sequestration of CO_2. II. Partitioning in chloride brines at 12-100 °C and up to 60 bar. Geochimica Cosmochimica Acta, 69 (13), 3309-3320.

Taku Ide, S., Jessen, K., Orr Jr, F. 2007. Storage of CO_2 in saline aquifers: Effects of gravity, viscous, and capillary forces on amount and timing of trapping. International Journal of Greenhouse Gas Control, 1 (4), 481-491.

Testamale, D., Dufaud, F., Martinez, I., Bénézeth, P., Hazemann, J. Schott, J., Guyot, F. 2009. An X-ray absorption study of the dissolution of siderite at 300 bar between 50°C and 100°C. Chemical Geology, 259 (1), 8-16.

U.S. Department of Energy, 2002. CO_2 capture and storage in geologic formations. A white paper prepared for the National Climate Change Technology Initiative.

van der Meer, L. 1993. The conditions limiting CO_2 storage in aquifers. Energy Conversion Management, 34 (9-11), 959-966.

Weir, G., White, S., Kissling, W. 1995. Reservoir storage and containment of greenhouse gases. Energy Conversion Management, 36 (6-9), 531-534.

Xu, T., Apps, J., Pruess, K. 2004. Numerical simulation of CO_2 disposal by mineral trapping in deep aquifers. Applied Geochemistry, 19 (6), 917–936.

Yang, D., Gu, Y., Tontiwachwuthikul, P. 2008. Wettability determination of the reservoir brine-reservoir rock system with dissolution of CO_2 at high pressures and elevated temperatures. Energy & Fuels, 22 (1), 504-509.

Zeng, Z. 2006. Multipurpose tri-axial core flooding system. Research Report. University of North Dakota, Grand Forks, ND, USA.

Zhou, Q., Birkholzer, J., Tsang, C., Rutqvist, J. 2008a. A method for quick assessment of CO_2 storage capacity in closed and semi-closed saline formations. International Journal of Greenhouse Gas Control, 2 (4), 626-639.

Zhou, X., Zeng, Z., and Belobraydic, M., Han, Y. 2008b. Geomechanical stability assessment of Williston Basin formations for petroleum production and CO_2 sequestration. 42nd US Rock Mechanics Symposium and 2nd U.S.-Canada Rock Mechanics Symposium, June 29-July 2, San Francisco, CA.

Zhou, X., Zeng, Z., Liu, H., Boock, A. 2009. Laboratory testing on geomechanical properties of carbonate rocks for CO_2 sequestration. 43rd US Rock Mechanics Symposium and 4th U.S.-Canada Rock Mechanics Symposium, June 28-July 1, Asheville, NC.